Unclassified
SECURITY CLASSIFICATION OF THIS PAGE

DTIC FILE COPY

(2)

AD-A223 321 DOCUMENTATION PAGE

Form Approved
OMB No. 0704-0188

Unclassified	1b. RESTRICTIVE MARKINGS: None
2a. SECURITY CLASSIFICATION AUTHORITY	3. DISTRIBUTION/AVAILABILITY OF REPORT: Distribution unlimited; approved for public release
2b. DECLASSIFICATION/DOWNGRADING SCHEDULE	
4. PERFORMING ORGANIZATION REPORT NUMBER(S)	5. MONITORING ORGANIZATION REPORT NUMBER(S): AFOSR-TR- 90 0686
6a. NAME OF PERFORMING ORGANIZATION: The Pennsylvania State Univ. / 6b. OFFICE SYMBOL (If applicable)	7a. NAME OF MONITORING ORGANIZATION: Air Force Office of Scientific Research
6c. ADDRESS (City, State, and ZIP Code): Mechanical Engineering Bldg. University Park, PA 16802	7b. ADDRESS (City, State, and ZIP Code): Building 410 Bolling AFB, DC 20332-6448
8a. NAME OF FUNDING/SPONSORING ORGANIZATION: Air Force Office of Sci. Res. / 8b. OFFICE SYMBOL (If applicable): AFOSR/NA	9. PROCUREMENT INSTRUMENT IDENTIFICATION NUMBER: AFOSR-87-0145
8c. ADDRESS (City, State, and ZIP Code): Building 410 Bolling AFB, DC 20332-6448	10. SOURCE OF FUNDING NUMBERS: PROGRAM ELEMENT NO. 61102F; PROJECT NO. 2308; TASK NO. A2; WORK UNIT ACCESSION NO.

11. TITLE (Include Security Classification)
"Fuel Structure and Pressure Effects on the Formation of Soot Particles in Diffusion Flames"

12. PERSONAL AUTHOR(S)
Robert J. Santoro

13a. TYPE OF REPORT	13b. TIME COVERED	14. DATE OF REPORT (Year, Month, Day)	15. PAGE COUNT
Annual	FROM 1/15/89 TO 1/15/90	1990 May 1	45

16. SUPPLEMENTARY NOTATION

17. COSATI CODES			18. SUBJECT TERMS (Continue on reverse if necessary and identify by block number)
FIELD	GROUP	SUB-GROUP	Soot Formation, Soot Particles, Diffusion Flames

19. ABSTRACT (Continue on reverse if necessary and identify by block number)

Studies emphasizing the effects of fuel concentration and operating pressure on the formation of soot particles have been conducted in a series of laminar diffusion flames. These experiments have shown that fuel concentration has a measurable effect on the amount of soot formed in the flame. However, a simple, constant proportionality between the fuel concentration and soot volume fraction has not been found to apply for the range of flow conditions studied. This observation is believed to be a result of flame residence time and diffusion effects which mitigate the consequences of reduced initial fuel concentration. Comparisons with simple laminar diffusion flame models are currently being used to investigate the relationship between initial fuel concentration and local flame concentration fields. Similar studies of soot formation in laminar diffusion flames as a function of operating pressure have also been completed for ethene, ethane and propene fuel species. In these studies, the pressure dependence of the maximum soot volume fraction formed in the flame has been represented as a power law, P^n, where P is the pressure. For the ethene case, n has been found to be 1.05±0.06 for a pressure range of 1 to 10 atm. Ethane, in contrast, has a somewhat higher value of n

20. DISTRIBUTION/AVAILABILITY OF ABSTRACT	21. ABSTRACT SECURITY CLASSIFICATION
☒ UNCLASSIFIED/UNLIMITED ☒ SAME AS RPT. ☐ DTIC USERS	Unclassified
22a. NAME OF RESPONSIBLE INDIVIDUAL: Julian M. Tishkoff	22b. TELEPHONE (Include Area Code): (202) 767-4935 / 22c. OFFICE SYMBOL: AFOSR/NA

DD Form 1473, JUN 86 — Previous editions are obsolete. — SECURITY CLASSIFICATION OF THIS PAGE

90 06 25 105

Unclassified

19. ABSTRACT (cont'd)

(1.62±.24) over a pressure range of 1 to 3 atm. Comparisons between the ethene studies and an ethane/propene mixture case has shown the that alkene fuels have similar values of n. The observed differences in the alkane and alkene results are presently being interpreted as a result of fuel molecular structure effects. Related efforts on the interpretation of optical properties of soot aggregates and the isolation of buoyancy effects in jet diffusion flames have also emerged from recent studies. Collaborative efforts with workers at Brown University and the National Institute of Standards and Technology are currently addressing these aspects of the present work.

Annual Report

on

Fuel Structure and Pressure Effects on the Formation of Soot Particles in Diffusion Flames

(AFOSR Contract AFOSR-87-0145)

Prepared by

Robert J. Santoro
Department of Mechanical Engineering
The Pennsylvania State University
University Park, PA 16802

Submitted to:

Air Force Office of Scientific Research
Bolling Air Force Base
Washington, D.C.

May 1990

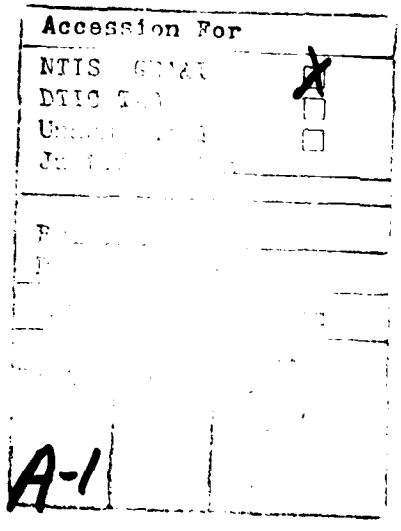

Table of Contents

Summary

Studies emphasizing the effects of fuel concentration and operating pressure on the formation of soot particles have been conducted in a series of laminar diffusion flames. These experiments have shown that fuel concentration has a measurable effect on the amount of soot formed in the flame. However, a simple, constant proportionality between the fuel concentration and soot volume fraction has not been found to apply for the range of flow conditions studied. This observation is believed to be a result of flame residence time and diffusion effects which mitigate the consequences of reduced initial fuel concentration. Comparisons with simple laminar diffusion flame models are currently being used to investigate the relationship between initial fuel concentration and local flame concentration fields. Similar studies of soot formation in laminar diffusion flames as a function of operating pressure have also been completed for ethene, ethane and propene fuel species. In these studies, the pressure dependence of the maximum soot volume fraction formed in the flame has been represented as a power law, P^n,where P is the pressure. For the ethene case, n has been found to be 1.05±0.06 for a pressure range of 1 to 10 atm. Ethane, in contrast, has a somewhat higher value of n (1.62±.24) over a pressure range of 1 to 3 atm. Comparisons between the ethene studies and an ethane/propene mixture case has shown the that alkene fuels have similar values of n. The observed differences in the alkane and alkene results are presently being interpreted as a result of fuel molecular structure effects. Related efforts on the interpretation of optical properties of soot aggregates and the isolation of buoyancy effects in jet diffusion flames have also emerged from recent studies. Collaborative efforts with workers at Brown University and the National Institute of Standards and Technology are currently addressing these aspects of the present work.

1. Research Objective

The objective of the present research program is to provide a fundamental understanding of the processes which control soot particle formation under conditions applicable to future gas turbine engine operation. In particular, the effects of fuel molecular structure and operating pressure are of interest. These parameters are viewed to be critical to the development of future gas turbine technology which will burn broad specification fuels at higher pressures. To achieve this objective, a fundamental study of the basic phenomena involved in soot particle inception, surface growth and oxidation is being conducted in well-controlled laminar diffusion flames. Through the understanding gained in these studies, improved prediction capabilities are expected to result which will impact the design methodology for future gas turbine combustors.

2. Research Approach

The basic nature of the objective of the present research program requires that fundamental studies be conducted under well controlled conditions. Additionally, a capability to provide extensive measurements of the soot particle, velocity, temperature and gas concentration fields is also desirable. For these reasons, the present studies are being conducted in a laminar diffusion flame environment burning in air to which a variety of diagnostic techniques are applied.

Fuel mixture studies employing a fuel addition approach have proven useful for the study of fuel molecular structure and pressure effects. In these studies, a well characterized methane or ethene baseline diffusion flame has been used. To these baseline flames, controlled amounts of an additional fuel species are added under conditions in which the total carbon atom flow rate is held constant. In this manner the effects of a particular fuel molecular structure can be investigated under similar flame conditions. These studies are carried out in a coannular diffusion flame configuration under both atmospheric and elevated pressure conditions. A high pressure diffusion flame facility capable of operating at pressures up to twenty atmospheres has been assembled for these high pressure studies. During the past year, investigations have been conducted for a pressure range of one to ten atmospheres.

Laser-based diagnostics have been emphasized in these studies for the soot particle and velocity field measurements. An extensive laser light scattering/extinction apparatus is utilized for the soot particle measurements. This apparatus has the capability to provide information on the volume fraction, particle diameter and number concentration of soot particles present in the flame. The extensive scattering measurements obtained as a function of scattering angle and laser polarization provide a redundant measurement capability to the extinction/scattering ratio technique also employed. These capabilities are useful in studies attempting to account for the aggregate nature of mature soot particles. Velocity measurements using a laser velocimetry technique are obtained to determine the particle paths and temporal history of the soot formation process. From the combined laser velocimetry and light scattering measurements, information on soot particle inception, surface growth and oxidation can be obtained.

These particle and velocity measurements are complemented by thermocouple measurements for temperature. Additionally, as part of the efforts during the last year, a quadrapole mass spectrometer and wavelength selective optical absorption system have been added to provide information on gas phase species present in these flames. These instruments will be used to determine species concentrations in future studies as well as to provide additional information on the soot particle properties in the inception region. Thus, the present approach utilizes carefully controlled experiments to which extensive diagnostic measurement techniques are applied to investigate basic mechanisms important in soot formation. Through this process, effects controlling the production and destruction of soot particles in combustion systems can be examined in a quantitative manner.

3. Research Accomplishments and Status of Work

During the past year, studies have concentrated on the effects of fuel concentration and operating pressure on the soot formation process. In addition, collaborative efforts with workers at other institutions (Brown University and NIST) have been undertaken to examine the optical properties of soot aggregates formed in the flame [1] and the effects of buoyancy in jet diffusion flames [2,3]. In addition to these studies, efforts have been made to enhance the diagnostic capabilities available for future studies. In particular, a quadrapole mass spectrometer system has been acquired and is presently operative. This instrumentation will be utilized to obtain information on gas phase species present in the flame and is intended to better characterize the particle inception and surface growth regions. Additionally, a spectroscopic absorption system has also been assembled to provide wavelength extensive information on both soot particles and large precursor species present in the flame.

High Pressure Diffusion Flame Studies

A series of laminar diffusion flames have been studied over a range of pressures between 1 and 10 atm (.1 MPa to 1.0 MPa). The coannular diffusion flame burner and laser diagnostics for soot particle measurements are similar to those used for atmospheric flame studies previously reported [4,5]. The coannular burner has been mounted in a high pressure cell which is extensively described elsewhere [6]. The studies undertaken involved laminar diffusion flames burning ethene (C_2H_4), ethane (C_2H_6) and a mixture of ethane and propene (C_3H_6) in air. The measured soot volume fraction is obtained from laser extinction measurements and is represented by [7]:

$$-\int_{-\infty}^{\infty} f_v \, dx = C(\lambda,m) \ln (I/I_o) \qquad (1)$$

where f_v is the local soot volume fraction, x lies along a laser path through the flame on a diameter D, $C(\lambda,m)$ is a constant which can be determined from Rayleigh light scattering theory to be 1.05×10^{-5} for m=1.57-0.56 i at λ=514.5nm [7], and finally I/I_o is the ratio of the transmitted to incident laser power. This quantity is proportional to the total soot present at a particular axial location in the flame. Figure 1 shows this quantity as a function of the non-dimensional axial location for the ethene/air flames at a series of operating pressures. If the increase in the maximum soot volume fraction at a particular operating pressure is related to that pressure through a power law dependence, that is

$$\left(\int f_v \, dx\right)_{max} \propto P^n \qquad (2)$$

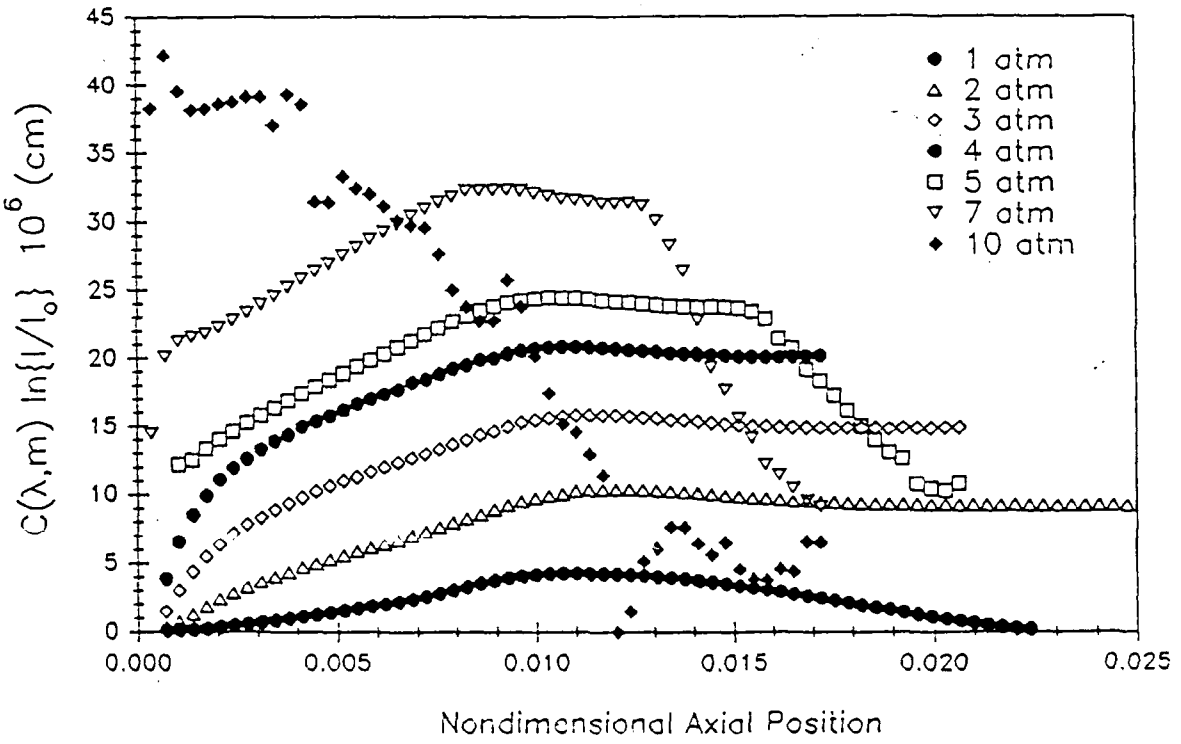

Figure 1. $C(\lambda,m)\ \ln (I/I_o)$ as a function of the non-dimensional position, η, for the ethene/air laminar diffusion flames for operating pressures between 1 and 10 atm. The non-dimensional axial position is given by $\eta=(zD/Q)\ \ln (1+1/s)$, where z is the axial position, D is the diffusion coefficient (0.156 cm^2s^{-1}), Q is the fuel flow rate (3.9 cm^3/s) and s is the volume of air to the volume of fuel required for complete combustion. (s=14.28 for C_2H_4).

then a fit to the data can be used to yield a value for n. Figure 2 shows the maximum soot volume fractions as a function of the operating pressure along with the best fit value for n determined from a linear least square procedure. For the ethene flame, the fuel flow rate was 3.9 cm^3/s and n was found to be 1.05±.06 in good agreement with the results of Flower and Bowman [7] who found n=1.2±0.1. It should be noted that results shown in Figures 1 and 2 have taken into account the slight burner diameter difference for the two studies. In the present study, the diameter was 1.1 cm where as Flower and Bowman employed a burner with a 1.27 cm diameter. Also shown on Figure 2 are the results for an ethene/air diffusion flame where a copper (Cu) rather than a stainless steel (SS) fuel tube was utilized. The results are very similar for both fuel tube materials. Although the higher heat loss characteristics of the copper fuel tube were observed to slightly reduce the amount of soot formed as compared to the stainless steel case, the pressure dependence is largely unaffected by the fuel tube material.

Figure 2 also shows the results obtained for flames burning ethane or an ethane/propene mixture. For these flames, the pressure could only be varied over a range of 1 to 3 atm (.1 to .3 MPa) before a buoyancy driven flame instability was observed. These buoyancy effects, at elevated pressure, have recently been the subject of a collaborative investigation with workers at the National Institute of Standards and Technology (NIST) [2,3] and are discussed elsewhere in this report. An analysis similar to that applied to the ethene flame studies yields pressure power dependences of n=1.88±0.13 and n=1.62±0.24 for ethane fuel flow rates of 2.80 and 3.85 cm^3/s, respectively. These higher values of the pressure power dependence appear to be related to fuel structure effects, the direct nature of which remains to be understood. These observations of a fuel structure dependence are consistent with previous studies [8].

As a further investigation of fuel molecular structure effects, a mixture of ethane (2.80 cm^3/s) and propene (0.7 cm^3/s) was studied and these results are also shown in Figure 2. In the ethane/propene study, the total carbon atom fuel flow rate was maintained constant with respect to the 3.85 cm^3/s ethane flame. For these conditions, the value of n is observed to be 1.16±0.10, a value similar to that observed for the ethene studies. Thus, the present studies with an alkane species appear to yield a higher pressure dependence than observed for either of the alkene species. This occurrence of a variation in the pressure dependence may be important in providing an understanding of the differences observed in premixed and diffusion flame studies at high pressure. For premixed flames, pressure dependence studies have yielded values of n=2 [9] as compared to the values of n between 1 and 1.2 reported for ethene. The higher values of n for the ethane flames are closer to the values observed in premixed flames. The cause of the higher pressure dependence obtained for the ethane diffusion flames remains to be established. Fuel structure effects may be reflected in the lower soot volume fractions rather than explicitly different chemical mechanisms. Premixed flame studies have examined a variety of fuels, including ethene and benzene, and

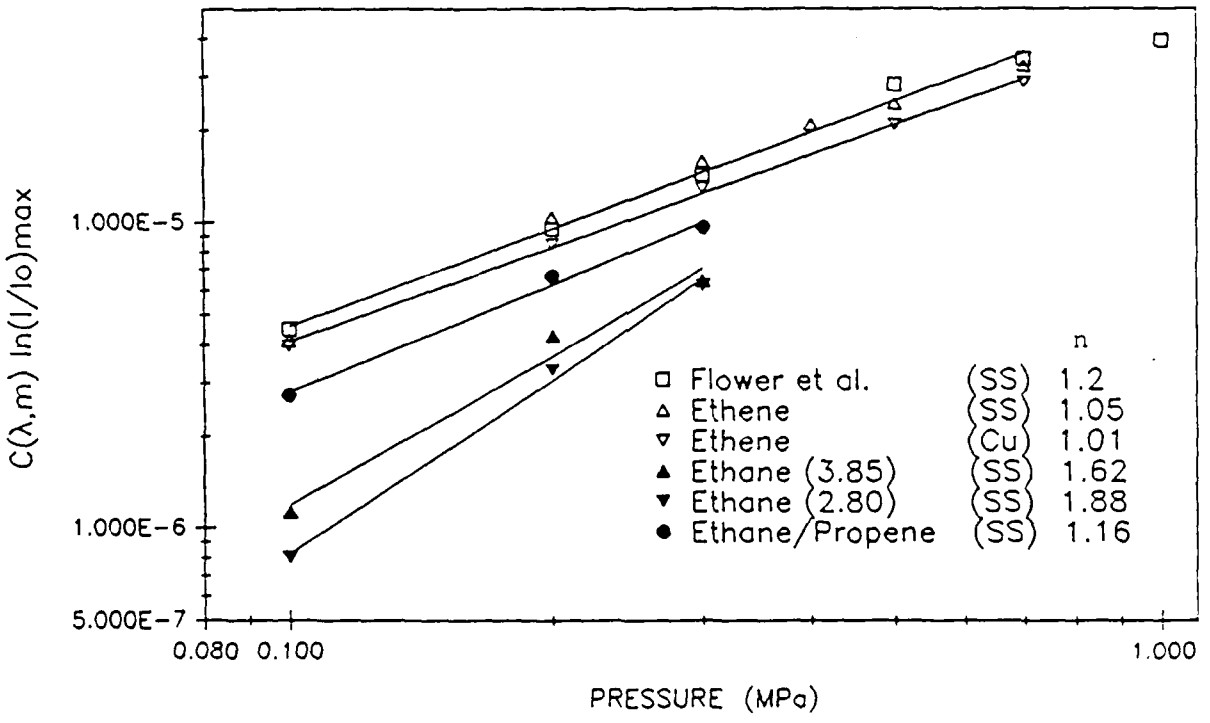

Figure 2. $C(\lambda,m)\ \ln\ (I/I_o)_{max}$ as a function of operating pressure for a series of ethene, ethane and ethane/propene laminar diffusion flames burning in air. Solid lines are fits to P^n.

obtained a P^2 dependence on pressure. However, the present experiments do provide some important additional information for consideration in resolving the actual pressure dependence for soot formation processes. Presently, consideration is being given to the likely sources for the observed differences as well as to extending the pressure range and fuel species considered for study.

Fuel Concentration Studies

Recently Axelbaum and Law [10] have examined the effects of fuel concentration and temperature on soot formation in a co-flow flame environment. Based on the importance of these results, a similar series of experiments have recently been undertaken in our laboratory. In these studies, fuel concentration and temperature are varied by the addition of nitrogen or argon to the fuel flow. Because of the difference in the heat capacity of these species, flames of identical calculated temperature but different fuel concentrations can be achieved. In the present studies, flames burning ethene and propane have been examined. The ethene flames have been studied for a range of fuel flow rates and dilutions while a single fuel flow rate condition has been examined for the propane flame (see Table 1).

In order to quantitatively determine the effect of variation in fuel concentration, the integrated soot volume fraction, F_v, was determined from the extinction measurements and is expressed as

$$-\frac{F_v}{k} = \int_{-\infty}^{\infty} \ln\left(\frac{I}{I_o}\right) dy \qquad (3)$$

where k is a constant and y is the axis perpendicular to the path of the laser beam. This measurement provides a quantity proportional to the soot volume fraction at a particular height integrated across the entire flame. In evaluating the effect of fuel concentration, the maximum value of F_v/k along the axial position was used. Values for F_v/k are tabulated in Tables 1 and 2 along with the fuel species, fuel flow rate, fuel mole fraction and the calculated adiabatic flame temperature for each diluent condition for the flames studied.

In order to quantify the effect of fuel concentration on the amount of soot formed in the flame, F_v/k was taken to be proportional to X_F^b for each temperature condition studied. From the observed differences in F_v/k for the nitrogen and argon dilution cases, a value for **b** could be obtained. For the flames of highest dilution (flames 1-4), **b** was equal to or exceeded 1. As the amount of dilution decreased (flames 5-10), **b** was observed to be 0.4 for the 4.9 cm^3/s fuel flow cases and 0.8 for the 6.58 cm^3/s fuel flow case. For the propane flame, **b** was also found to be 0.4. No systematic variation in the value of **b** was evident with respect to fuel flow rate. These observations in general reaffirm the earlier results of Axelbaum and Law with regard to the importance of concentration [10]. However, the deviation of **b** from unity indicates that other effects such as residence time or diffusion may also be important.

As an alternative approach to studying concentration effects, a 50% argon diluted propane or

TABLE 1

Experiment #	Fuel (Q) (cm^3/s)	Diluent	X_{Fuel}	T_{ad} (K)	(F_v/k)	% of Pure $(F_v/k)/(F_v/k)_{Pure}$
1	C_2H_4(2.75)	N_2	0.50	2310	0.0244	46.7
2	C_2H_4(2.75)	Ar	0.37	2310	0.0155	29.6
3	C_2H_4(4.90)	N_2	0.50	2310	0.0429	51.8
4	C_2H_4(4.90)	Ar	0.37	2310	0.0312	37.7
5	C_2H_4(4.90)	N_2	0.74	2346	0.0722	87.2
6	C_2H_4(4.90)	Ar	0.64	2346	0.0672	81.2
7	C_2H_4(4.90)	N_2	0.64	2333	0.0602	72.7
8	C_2H_4(4.90)	Ar	0.52	2333	0.0556	67.2
9	C_2H_4(6.58)	N_2	0.64	2333	0.0781	74.5
10	C_2H_4(6.58)	Ar	0.52	2333	0.0660	63.0
11	C_2H_4(2.75)	--	1.00	2369	0.0522	100.0
12	C_2H_4(4.90)	--	1.00	2369	0.0828	100.0
13	C_2H_4(6.58)	--	1.00	2369	0.1047	100.0
14	C_3H_8(2.56)	N_2	0.61	2240	0.0392	79.8
15	C_3H_8(2.56)	Ar	0.50	2240	0.0362	73.7
16	C_3H_8(2.56)	--	1.00	2266	0.0491	100.0

TABLE 2

Experiment #	Fuel (Q) (cm^3/s)	Diluent	Pressure (atm)	X_{Fuel}	T_{ad} (K)	(F_v/k)
17	C_2H_4(3.85)	--	1	1.00	2369	0.0767
18	C_2H_4(3.85)	Ar	2	0.50	2351	0.0959
19	C_3H_8(2.56)	--	1	1.00	2260	0.0490
20	C_3H_8(2.56)	Ar	2	0.50	2258	0.0780

ethene flame at two atmospheres operating pressure was investigated and compared to appropriate undiluted flames at a pressure of one atmosphere. For these conditions, the initial molar fuel concentrations are the same for the flames at each pressure. The results for these studies are shown in Table 2. Clearly, the amount of soot formed increases in the two atmosphere flames indicating that effects in addition to the fuel concentration are enhancing the formation of soot as the operating pressure increases.

The above results are presently being further analyzed to assess the importance of residence time and diffusion on the observed concentration effects. Of particular interest is the importance of concentration versus temperature on the early particle inception region. This aspect of the study will likely require information on the gas phase species present in the flame, which is a major focus of future studies. However, present analysis is using an approach based on comparisons with an existing diffusion flame model [11]. In these comparisons, the concentration of fuel and oxidizer species are calculated as a function of initial fuel concentration and position in the diffusion flame. The analysis indicates that diffusion processes do rapidly alter the concentration field mitigating to a degree the effect of dilution of the fuel. Thus, the lower dependence of the soot volume fraction on the fuel concentration could reflect this diffusion effect. The comparison between these detailed measurements of the soot formation processes and model prediction is viewed as a very fruitful approach to resolving the observed effects of temperature and concentration.

Light Scattering Properties of Soot Aggregates

Light scattering measurements have become an important measurement approach for determining soot particle size and volume fraction in flames [1,4]. However, most optical measurement interpretations rely on the presence of spherical soot particles. For mature soot particles, which have undergone extensive coagulation and aggregation processes, deviations from a spherical geometry are likely. One approach to examining such effects involves a fractal geometry interpretation of the aggregate particle structure. From such a treatment, information on the particle size and concentration can be obtained using light scattering measurements obtained at several angles (e.g. 45°, 90° and 135°) along with extinction measurements. Recently, a collaborative effort with Prof. R. Dobbins of Brown University to apply such an analysis approach has been undertaken using light scattering measurements obtained in the present laminar diffusion flame studies [1]. These studies, which are presented in detail in attachment 1, have revealed that the proper treatment of the aggregate nature of mature soot particles can be addressed in the present studies. Accounting for aggregates has been shown to be important in the accurate prediction number concentration, particle size and surface area [1]. Additionally, extensive comparisons between the aggregate analysis approach and experimental data has led to speculation concerning the importance of variations in the refractive index on the measured soot particle properties. Presently, additional comparisons between the aggregate theory and diffusion flame measurements are being pursued, since it is felt that the

aggregate theory may provide a simple approach for accounting for non-spherical particle effects. Once this conclusion is fully substaniated, a wide range of optical measurements of particle properties are likely to be affected.

Buoyancy Effects in Jet Diffusion Flames

The occurrence of instability phenomena in flames has been a topic of interest in combustion for a variety of reasons. Instability processes have been observed to enhance mixing and, thus, accelerate chemical reaction progress. Less favorable results have been observed to accompany combustion instabilities as well. For gas turbine and rocket engines, combustion instabilities can present serious operational problems and may, in fact, lead to catastrophic engine failure. In such cases, expensive engine redesign or implementation of damping devices has been necessary to resolve the problem. Clearly, a desirable situation would be one in which the potential benefits to enhanced mixing could be realized without the penalties of hardware performance loss. This requires a fundamental understanding of phenomena which controls the initiation and growth of the instability. One of the obstacles to achieving such an understanding lies in the inability to study instability phenomena under well controlled conditions.

In addition to the combustion instability interests, turbulence combustion phenomena may also be influenced by instability phenomena. The occurrence of well ordered structures in turbulent flames has been a subject of great interest over the preceeding decade. Although often observed, the importance of such features with respect to the transition to turbulent combustion conditions is still an area of active investigation. An understanding of the basic mechanisms controlling the onset of these structures is still lacking.

Recently, an interesting flame instability phenomena was observed during the study of soot formation in high pressure diffusion flames which possesses many of the desired features for the study of this phenomena. The flame instability was observed to evolve from a stable methane/air diffusion flame as the pressure was raised from one atmosphere (14.7 psia) to approximately 6 psig (20.7 psia). At this pressure, the flame exhibited a regular pulsation or oscillation. In order to examine this phenomena further, a series of high speed video images of this methane flame were recorded. These images were obtained at a framing rate of 500 frames per second and simply recorded the flame luminosity from the soot present in the flame. Analysis of these video recordings revealed the onset and evolution of a very regular flame structure with a repetition rate of approximately 15 Hz. Several attempts were made to eliminate these pulsating flames by modifying the pressure chamber with baffles or screens. These changes were intended to alter the acoustic modes of the chamber or to impede flow recirculation. None of these approaches significantly affected the phenomena. Thus, the observed oscillations are not believed to be an artifact of the apparatus.

Previous researchers have observed similar self-excited instabilities in laminar fuel jets [12,13].

In these studies, the fuel flow rate was varied to produce the onset of the instability. Analysis explaining the oscillatory behavior emphasized perturbations introduced into the velocity field which were amplified through either linear or non-linear mechanisms [12,13]. More recent work has placed a stronger emphasis on the effect of buoyancy in both laminar and turbulent flow regimes [14,15-18]. The general trends indicate that as Reynolds number increases (Re>7000), the effect of these buoyancy related instabilities is less important [14,18]. The present evidence is not conclusive on the potential importance of such low frequency instabilities with regard to turbulent flows. There are studies which indicate that the above observed instabilities can couple to the inner core flow of the jet and may be important in the dynamic processes which occur during transition to fully turbulent conditions [14,17]. Recent visualization studies of atmospheric pressure diffusion flames have shown that these flames are characterized by complex vortical structures [17].

The general flame structure of these high pressure oscillating flames is similar to that reported in the studies referenced in the above discussion. The observed frequency is quite close to the 17 Hz frequency predicted by the analysis of Buckmaster and Peters [15]. Thus, it seems clear that these instability features are buoyancy driven. Recent modelling results for unsteady buoyancy-driven jet diffusion flames conducted at NIST have been quite successful in reproducing the general characteristics of the observed flames [2,3]. In the formulation of this model, three dimensionless parameters enter into the formulation: the Reynolds number, the Peclet number and the Richardson number. In the present experiments, because the mass flow rates of fuel and oxidizer are maintained at a constant value, the product of the density and inlet gas velocity remains constant as the pressure is changed. Since the viscosity is independent of the pressure, the Reynolds number also remains constant as the pressure is varied. In the limit of unity Lewis number, the Peclet number is equal to the fuel jet radius multiplied by the ratio of inlet gas velocity and the binary diffusion coefficient of the fuel. Since both the inlet gas velocity and the diffusion coefficient are inversely proportional to the pressure, the Peclet number also remains constant. Finally, the Richardson number, which expresses the ratio of buoyancy forces to inertial forces, can be expressed as gL/U^2 where g is the gravitational constant, L is the fuel jet radius and U is taken as the air inlet velocity. Clearly, this number will vary with the square of the pressure through the velocity term in this ratio. Thus, the effective gravitational acceleration will vary as the pressure squared. Consequently, in the model, a pressure of two atmospheres can be simply simulated by choosing a gravitational constant of 4 g.

The significance of the present experimental configuration is that relative effects of buoyancy can be examined in isolation from the other parameters. This situation is unique to this burner configuration and offers an excellent opportunity for investigating the fundamental aspects of the instability onset from both experimental and theoretical modelling aspects.

Preliminary model comparisons with the imaging results described above show good agreement with respect to the instability frequency and tip cutting location [2,3]. This agreement includes the

predication of the observation that the tip cutting location decreases as the pressure increases. One area where agreement has not been obtained to date, involves the pressure at which the onset of the instability is observed. The model predicts a pressure of about one half that observed experimentally. Attachment 2 contains a detailed discussion of the model and experiment comparisons [3].

Additional experiments using ethane and ethene have also displayed similar flame instability behavior as the pressure is increased. For each flame, however, the onset of the instability occurs at distinctly different pressures, even though the gas flow rates are identical. Thus, a measurable fuel dependence is observed with respect to the onset conditions. Previous studies at atmospheric conditions have not investigated fuel related effects, because the instability frequency generally is not strongly affected [15]. For the high pressure initiated instabilities, however, measurable fuel constituent effects are observed and, thus, provide a potential for further insights into the instability phenomena.

4. Future Work

The results described in the preceding sections have considered several important parameters which affect the formation of soot particles and their measurements in combustion systems. Present efforts are directed at combining the recent results on fuel concentration and pressure effects with previous work considering surface growth and fuel molecular structure effects. These latter two subjects are presently the focus of two papers which are in preparation. Both of these papers will be submitted for publication shortly.

Further analysis of fuel concentration effects is being pursued using a comparison with an existing diffusion flame model [11]. These comparisons will soon be complemented with gas species concentration measurements in diluted flames obtained with the quadrapole mass spectrometer facility mentioned earlier. The objective of these measurements is to quantify the effects of diffusion on the diluted fuel flow cases in terms of the actual concentration profiles achieved in the flame. It is felt that this information will help resolve the explanation of the observed dependence of the soot volume fraction on the initial fuel concentration. The present results indicate the proportionality between the soot volume fraction observed in the flame and the fuel concentration varies as fuel concentration and fuel species are changed.

Future directions for the current research effort will emphasize soot particle and gas species measurements in and near the soot particle inception zone. Previous studies of the surface growth process indicate that this region is critical in determining the amount of soot formed in the flame. Mass spectrometric and optical absorption measurements are to be emphasized to provide additional information on soot precursor species and surface growth reactants. To accomplish these goals, novel gas sampling approaches are currently under development to provide for sampling in particle laden fuel-rich regions. Finally, a continued effort will be maintained with respect to the interpretation of optical measurements of soot particles as well as the effects of buoyancy in jet diffusion flames.

5. References

1. Dobbins, R.A., Santoro, R.J. and Semerjian, H.G., "Analysis of Light Scattering from Soot Using Optical Cross Sections for Aggregates", Twenty-Third Symposium (International) on Combustion, accepted for publication (1990).

2. Davis, R.W., Moore, E.F., Santoro, R.J. and Ness, J.R., "Isolation of Buoyancy Effects in Jet Diffusion Flames", presented at the Central States Section, The Combustion Institute, Cincinnati, OH, May 20-22, 1990.

3. Davis, R.W., Moore, E.F., Santoro, R.J. and Ness, J.R., "Isolation of Buoyancy Effects in Jet Diffusion Flames", Submitted to Combustion Science and Technology.

4. Santoro, R.J., Yeh, T.T., Horvath, J.J. and Semerjian, H.G., "Soot Particle Measurements in Diffusion Flames", Combustion Science and Technology, 53, 89 (1987).

5. Richardson, T.F. and Santoro, R. J., "Soot Growth in Diffusion Flames Burning Fuel Mixtures", 1988 Fall Technical Meeting of the Eastern States Section of the Combustion Institute, Clearwater Beach, FL, Dec. 5-7, 1988.

6. Santoro, R.J., "Fuel Structure and Pressure Effects on the Formation of Soot Particles in Diffusion Flames", Annual Report, Air Force Office of Scientific Research, AFOSR Contract AFOSR-87-0145, March 1989.

7. Flower, W.L. and Bowman, C.T., "Soot Production in Axisymmetric Laminar Diffusion Flames at Pressures from One to Ten Atmospheres", Twenty-first Symposium (International) on Combustion, The Combustion Institute, pp. 1115-1124 (1986).

8. Schalla, R.L., Clark, T.P. and McDonald, G.E., "Formation and Combustion of Smoke in Laminar Flames", NACA Report 1186 (1954).

9. Bohm, H., Hesse, D., Jander, H., Luers, B., Pietscher, J., Wagner, H.Gg. and Weiss, M., "The Influence of Pressure and Temperature on Soot Formation in Premixed Flames," Twenty-second Symposium (International) on Combustion, The Combustion Institute, pp. 403-411 (1988).

10. Axelbaum, R.L. and Law, C.K., "Dilution and Temperature Effects on Soot Formation in the Co-Flow Flame", The Eastern Section of the Combustion Institute, Fall Technical Meeting, paper 60, Albany, NY, Oct. 30, 31 and Nov. 1, 1989.

11. Mitchell, R.E., Sarofim, A.F. and Clomburg, L.A., "Experimental and Numerical Investigation of Confined Laminar Diffusion Flames," Combustion and Flame, 37, pp. 227-244 (1980).

12. Kimura, I., "Stability of Laminar-Jet Flames", Tenth Symposium (International) on Combustion, The Combustion Institute, pp. 1295-1300 (1965).

13. Toong, T.T., Salant, R.F., Stopford, J.M. and Anderson, G.Y., "Mechanisms of Combustion Instability", Tenth Symposium (International) on Combustion, The Combustion Institute, pp. 1301-1313 (1965).

14. Coats, C.M. and Zhao, H., "Transition and Stability of Turbulent Jet Diffusion Flames," Twenty-second Symposium (International) on Combustion, The Combustion Institute, pp. 685-692 (1988).

15. Buckmaster, J. and Peters, N., "The Infinite Candle and Its Stability - A Paradigm for Flickering Diffusion Falmes", Twenty-first Symposium (International) on Combustion, The Combustion Institute, pp. 1829-1836 (1986).

16. Lewis, G.S., Cantwell, B.J., Vandsburger, U. and Bowman, C.T., "An Investigation of the Structure of a Laminar Non-Premixed Flame in an Unsteady Vortical Flow", Twenty-second Symposium (International) on Combustion, The Combustion Institute, pp. 515-522 (1988).

17. Chen, L.-D., Seaba, J.P., Roquemore, W.M. and Goss, L.P., "Buoyant Diffusion Flames", Twenty-second Sympsoium (International) on Combustion, The Combustion Institute, pp. 677-684 (1988).

18. Ballantyne, A. and Bray, K.N.C., "Investigations into the Structure of Jet Diffusion Flames Using Time-resolved Optical Measurement Techniques", Sixteenth Symposium (International) on Combustion, pp. 777-787 (1976).

6. Publications

1. Santoro, R. J., Yeh, T. T., Horvath, J. J. and Semerjian, H. G., "The Transport and Growth of Soot Particles in Laminar Diffusion Flames," Combustion Science and Technology, 53, 89 (1987).

2. Solomon, P. R., Best, P. E., Carangelo, R. M., Markham, J. R., Chien, P., Santoro, R. J. and Semerjian, H. G., "FT-IR Emission/Transmission Spectroscopy for In-Situ Combustion Diagnostics", Twenty-first Symposium (International) on Combustion, The Combustion Institute, pp. 1763-1771 (1986).

3. Santoro, R. J. and Miller, J. H., "Soot Particle Formation in Laminar Diffusion Flames", Langmuir, 3, p. 244-254 (1987).

4. Santoro, R. J., "Optical Measurements of Soot Particles in Flames," Mat. Res. Soc. Symp. Proc., Vol. 117, p. 157 (1988).

5. Dobbins, R.A., Santoro, R.J. and Semerjian, H.G., "Analysis of Light Scattering from Soot Using Optical Cross Sections for Aggregates", Twenty-Third Symposium (International) on Combustion, accepted for publication (1990).

6. Davis, R.W., Moore, E.F., Santoro, R.J. and Ness, J., "Isolation of Buoyancy Effects in Jet Diffusion Flames", submitted to Combustion Science and Technology.

7. Meetings and Presentations

1. "The Effect of Fuel Structure on the Formation and Growth of Soot Particles in Diffusion Flames," The Twenty-third Biennial Conference on Carbon, Worcester Polytechnic Institute, July 19-24, 1987.

2. "Soot Particle Formation in Diffusion Flames," American Chemical Society Symposium on Advances in Soot Chemistry, ASC Symposium, New Orleans, LA, August 30-September 4, 1987.

3. "Fuel Molecular Structure Effects on Soot Particle Growth in Diffusion Flames", Twentieth Fall Technical Meeting of the Eastern Section of the Combustion Institute, Gaithersburg, MD, November 2-5, 1987.

4. "Optical Measurements of Soot Particles in Flames," Materials Research Society Symposia, Reno, Nevada, April 5-8, 1988.

5. "Soot Growth in Diffusion Flames Burning Fuel Mixtures," 1988 Fall Technical Meeting of the Eastern Section of the Combustion Institute, Clearwater Beach, FL, December 5-7, 1988.

6. "Optical Measurements of Soot Particles in Flames," Wright Patterson Air Force Base, Dayton, Ohio, March 6, 1989.

7. Invited Attendee for the Round Table Discussion on "Current Problems in Soot Formation During Combustion," The Commission on Condensation Phenomena of the Academy Science, Gottingen, Germany, March 29 and 30, 1989.

8. *Invited Tutorial on Particle Diagnostics*, 1989 Annual Meeting of the American Association for Aerosol Research, Reno, Nevada, October 9, 1989.

9. "Surface Growth and Coagulation Processes in Soot Particle Formation," AIChE Annual Meeting, San Francisco, CA, November 6-10, 1989.

10. "Isolation of Buoyancy Effects in Jet Diffusion Flames," presented at the 1990 Central States Section of the Combustion Institute, Cincinnati, OH, May 20-22, 1990.

8. Participating Professionals

Dr. Robert J. Santoro, Associate Professor of Mechanical Engineering
Mr. Rahul Puri, Graduate Student, Department of Mechanical Engineering (Ph.D. expectd 8/91)
Mr. Jeff Leet, Graduate Student, Department of Mechanical Engineering (M.S. completed 8/90, presently employed at Southwest Research Institute)
Mr. Thomas Richardson, Graduate Student, Department of Mechanical Engineering (Ph.D. expected 8/91)
Mr. John Ness, Graduate Student (AFRAPT), Department of Mechanical Engineering (M.S. completed 8/90, to be employed at David Taylor Laboratory)
Mr. Robert Burch, Graduate Student (AFRAPT), Department of Mechanical Engineering

9. Interactions

A number of researchers have directly used the extensive data set developed as part of this work to compare with or extend their own research. Some of those who have been directly provided data include:

Professor R. A. Dobbins, Brown University, Providence, RI
Dr. R. Hall, United Technologies Research Center, East Hartford, CT
Dr. R. Davis, The National Bureau of Standards, Gaithersburg, MD
Dr. P. Solomon, Advanced Fuel Research, Inc., East Hartford, CT
Dr. I. Kennedy, University of California, Davis, CA
Drs. C. Merkle and S. Turns, The Pennsylvania State University, University Park, PA

In addition to the interactions resulting from interest in the soot particle data, there have been interactions with researchers on particle diagnostic problems. In some cases this has resulted in direct visits to particular laboratories to assist in solving these problems. These interactions include:

Dr. M. Zachariah, The National Bureau of Standards, Gaithersburg, MD
Dr. Valerie Lyons, NASA-Lewis Research Center, Cleveland, OH

Several other interactions have also occurred through a general interest in the work supported by AFOSR with:

Columbian Chemical Company, Monroe, LA
Cummins Engine Company, Columbus, IN
E. I. DuPont de Nemours, Wilmington, DE

DuPont is currently supporting work on titanium dioxide particle formation as a direct result of the AFOSR research program. A student, Peter Strakey, will spend the summer with DuPont exchanging expertise and technology developed as part of this research.

Attachment 1

Analysis of Light Scattering from Soot Using Optical Cross Sections for Aggregates
by
R. A. Dobbins, R. J. Santoro and H. G. Semerjian

accepted for publication in the Twenty-Third Symposium (International) on Combustion

ANALYSIS OF LIGHT SCATTERING FROM SOOT USING OPTICAL CROSS SECTIONS FOR AGGREGATES

R. A. Dobbins, Division of Engineering
Brown University
Providence, RI 02912.

R. J. Santoro, Department of Mechanical Engineering
The Pennsylvania State University
University Park, PA 16802.

and

H. G. Semerjian, Center for Chemical Technology
National Institute of Standards and Technology
Gaithersburg, MD 20899.

Abstract

Soot formed in flames usually consists of aggregates (clusters or agglomerates) of a variable number of nearly spherical, monodisperse primary particles (monomers or spherules). In this work, the optical properties of polydisperse aggregates are used to analyze light scattering data from a coannular ethene diffusion flame. In previously reported studies, data have been obtained on the local extinction and volumetric scattering cross sections from laser scattering experiments, on the flame velocity field from laser velocimetry, and on the primary particle sizes determined by electron microscopy. The present analysis yields the average number of primary particles per aggregate, the mean-square radius of gyration, the average number of primary particles per aggregate, the soot volume fraction, and the aggregation rate. It is found that sustained collisional growth of the aggregates occurs while their primary particles grow through heterogeneous reactions low in the flame, and contract through surface oxidation in the upper half of the flame. A recent value of the refractive index gives internally consistent moment ratios of the aggregate size distribution function. This method of analysis provides a more detailed and complete description of the formation, growth and oxidation of soot aggregates in a diffusion flame.

Subject: Soot Formation, Laminar Diffusion Flames

Introduction

The use of laser light scattering experiments to probe the development of the soot field in the coannular laminar ethene diffusion flame has been previously reported[1]. This work was based on the progress made by various investigators to measure the optical properties of the soot particle field with high spatial resolution[2,3,4] and the application of a tomographic inversion technique[5] to obtain local values of the extinction coefficient for axisymetric diffusion flames. The measured extinction and volumetric scattering cross sections were introduced into expressions derived from the Rayleigh description for the scattering of light by small spheres. Polydispersity was included by assuming the size distribution to be self preserving. However, Rayleigh theory implies that the vertically polarized component of scattering is independent of the scattering angle Θ measured from the forward direction. This condition is not fulfilled in the annular region of the flame where high soot concentrations were observed and the scattering in the forward direction was more pronounced.[6]

Subsequently a detailed mapping of the flame velocity and temperature fields[7] provided information on the soot transport and growth processes. Information on particle morphology was also developed[8] by means of a thermophoretic sampling technique. These results showed the soot particles in the ethene diffusion flame to consist of aggregates of primary particles whose shape was approximately spherical and whose diameters d_p in any one flame location was quite uniform. The optical properties of aggregates was further studied through computational simulation[9] of both the cluster-cluster growth and the light scattering processes. These results together with the observations of the soot field by electron microscopy (TEM)[10,11,12] were used to formulate[13] the optical cross sections of polydisperse aggregates. Polydispersity results when the number n of primary particles per aggregate is variable within a given aggregate population, and is the inevitable result of the cluster-cluster aggregation process.

These developments now make possible the analysis of the measured optical properties of soot using the cross sections for randomly-oriented aggregates. The presence of angular dissymmetry of the scattered light provides the opportunity to perform a more detailed study than would otherwise be possible. Additionally, the accumulated data on this flame - scattering and extinction measurements,

velocity data from laser Doppler anemometry, and primary particle sizes as determined by TEM - in the region of maximum soot concentration allow for a detailed examination of the dynamics of the processes which influence the soot field. In particular, with the development of an aggregate model for the optical cross sections, the effects of the aggregation process on particle morphology, surface area and number concentration can be investigated. The combination of detailed optical measurements along with an aggregate-based analysis provides an improved understanding into the evolution of soot particle fields in flames. Given the recent interest in the modeling of the formation and growth of soot particles and their relationship to flame radiation, improved approaches for the interpretation of optical measurements of soot aggregates is a topic of significant importance.

Theoretical Background

I. Aggregate Statistics

A single aggregate is characterized by the primary particle diameter d_p, the number of primary particles within the aggregate n, and its radius of gyration R_g *that is given by*

$$R_g^2 = \frac{1}{n} \sum_i r^2 \qquad (1)$$

where r_i is the distance of the ith primary particle to the center of mass of the aggregate. Large aggregates are mass fractals[14,15,16] which display scale similarity and obey the relationship

$$n = k_f \left[\frac{R_g}{d_p} \right]^{D_f} \qquad (2)$$

where k_f is the prefactor and D_f is the fractal or Hausdorf dimension. When aggregates grow by cluster-cluster collision processes, the fractal dimension is in the range of 1.7 to 1.9. Although Eq. (2) applies to a population of particles on a statistical basis, even relatively small aggregates ($n \approx 5$) that do

not display scale similarity have been found to follow this relationship.[12]

In order to describe a population of aggregates, it is necessary to introduce the probability distribution function (PDF) p(n) that represents the relative frequency of occurrence of aggregates containing n primary particles. The q^{th} moment of the PDF is given by

$$\overline{n^q} = \sum_n n^q \, p(n) \tag{3}$$

Furthermore, for each value of n there is an associated volume-equivalent diameter D and, for the total aggregate population, the corresponding volume-mean diameter D_{30} is given[12] by

$$D_{30}^3 = d_p^3 \, \overline{n^1} \tag{4}$$

where $\overline{n^1}$ is the average number of primary particles per aggregate. Since the diameters of the primary particles in a given region of a laminar flame are narrowly distributed (see Ref. 12 and the references cited therein), in this work we treat the primary particles as monodisperse at each flame location. With this definition, the volume fraction f_v of an aerosol of N_a aggregates per unit volume can be expressed as

$$f_v = \frac{\pi}{6} D_{30}^3 N_a . \tag{5}$$

The volume fraction is a quantity for which optical techniques provide direct information and is a primary quantity of interest in the present analysis.

Finally a series of relationships exist relating primary and aggregate particle properties to each other and to important observables. A moment ratio that is important in the reduction of light scattering data is f_n, which is a measure of the width of the PDF, and is defined by

$$f_n = \frac{\overline{n^2}}{(\overline{n^1})^2} \quad . \tag{6}$$

For monodisperse aggregates f_n is unity and it attains a value near 2.0 for the continuous self preserving distribution function. This quantity explicitly enters into the analysis of light scattering measurements for determining D_{30} which is described in the next section.

The number of primary particles per unit volume can be related to the number of aggregates by

$$N_p = \overline{n^1}\ N_a \tag{7}$$

and the surface area per unit volume S_t can be calculated if it is assumed that the primary particles are in point contact with one another, yielding

$$S_t = \pi\ d_p^2\ \overline{n^1}\ N_a \quad . \tag{8}$$

Since surface growth leads to the formation of menisci that reduce the surface area, the value of S_t yielded by Eq. (8) is an upper bound estimate. A population of polydisperse aggregates has a mean-square radius of gyration $\overline{R_g^2}$ that is defined by weighting $R_g^2(n)$ by n^2, see Appendix I. The final important relationship relates the mean-square radius of gyration $\overline{R_g^2}$ with d_p and D_{30}.

$$d_p = \frac{D_{30}^3}{\overline{\kappa}\ \overline{R_g^2}} \tag{9}$$

where $\overline{\kappa}$ is a high moment ratio of the PDF defined in Appendix I.

The above equations contain eight properties relevent to the description of a suspension of aggregates - d_p, D_{30}, f_v, N_a, N_p, $\overline{n^1}$, $\overline{R_g^2}$, and S_t. As five algebraic relationships exist, [Eqs. (4), (5), (7), (8) and (9)] and, if f_n, $\overline{\kappa}$ and D_f are known, there are three degrees of freedom. Measurements of three optical properties which are independent functions of three or more of the above eight properties are required to completely specify the aggregate population when the refractive index of the aggregate

material is known. In the procedure employed below, we will consider f_n and $\bar{\kappa}$, which are not independent, as unknown and will use, as substitute information, a determination of d_p by TEM.

II. Optical Properties of Aggregates

The extinction coefficient for aggregates which both absorb and scatter light[13] is given by

$$K_{ext}^{A} = \frac{4\pi N_a \overline{n^1} \; x_p^3 E(m)}{k^2} (1 + \overline{\rho_{sa}}) \tag{10}$$

where

$$E(m) = -Im\left[\frac{m^2-1}{m^2+2}\right] \tag{11}$$

with $x_p = \pi d_p/\lambda$, $k = 2\pi/\lambda$, $m = m_1 - im_2$ is the refractive index, and $\overline{\rho_{sa}}$ is the ratio of the scattering to absorption cross sections for the population of polydisperse aggregates.[13] The determination of $\overline{\rho_{sa}}$, which is often small but is significant at midflame heights in the ethene diffusion flame, is given in Appendix II.

Because the product of $\overline{n^1}$, d_p^3, and N_a appears in Eq. (10), the particle volume fraction is directly obtainable from a measurement of extinction without any requirement of knowledge of the size distribution function. By combining Eqs. (5) and (10), we find the particle volume fraction,

$$f_v = \frac{K_{ext}^{A}}{3k\,E(m)\,(1+\overline{\rho_{sa}})} = \frac{K_{abs}^{A}}{3k\,E(m)} \tag{12}$$

The volumetric scattering cross section $Q_{vv}^{A}(\Theta)$ for vertically polarized scattered light, when the incident beam is also vertically polarized with respect to the scattering plane, is the product of N_a and the mean cross section of the aggregates[13]. It is given by

$$Q_{VV}^{A}(\Theta) = \frac{N_a \overline{n^2} \; x_p^6 \, F(m)}{k^2} f(q_i^2 \, \overline{R_g^2}) \tag{13}$$

with

$$F(m) = \left| \frac{m^2 - 1}{m^2 + 2} \right|^2 \tag{14}$$

and q_i is the modulus of the scattering vector defined by

$$q_i = \frac{4\pi}{\lambda} \sin \frac{\Theta_i}{2} \; . \tag{15}$$

The function $f(q_i^2 \, \overline{R_g^2})$ results from the examination of the angular scattering of light by aggregates[13] whose its functional form depends on $q_i^2 \, \overline{R_g^2}$ and D_f as summarized below. For small and intermediate sizes, $q_i^2 \, R_g^2 < 1.5 \, D_f$, the function $f(q_i^2 \, \overline{R_g^2})$ is given by

$$f(q_i^2 \overline{R_g^2}) = \exp\left[- \frac{q_i^2 \, \overline{R_g^2}}{3} \right] \tag{16}$$

while for larger sizes, $q_i^2 \overline{R_g^2} > 1.5 \, D_f$, the following expression applies,

$$f(q_i^2 \overline{R_g^2}) = \frac{C_p}{(q_i^2 \overline{R_g^2})^{D_f/2}} \tag{17}$$

where $C_p = (1.5 \, D_f/e)^{D_f/2} = 0.9939$ for $D_f = 1.80$ as is representative for cluster-cluster aggregation. Equations (16) and (17) result from the detailed investigation[13] of the influence of polydispersity on the optical properties of randomly oriented aggregates, and they are related to expressions which appear in the literature of fractals[14,15,16]. The inclusion of the effects of polydispersity of the aggregates is an imperative consideration in understanding the soot formation processes in flames.

The mean-square radius of gyration, $\overline{R_g^2}$, is directly yielded by solving Eqs. (13), (16) and (17) as appropriate for the ratio $R_{ij} = Q_{VV}^{A}(\Theta_i)/Q_{VV}^{A}(\Theta_j)$, which depends only on $k^2 \, \overline{R_g^2}$ for specified values of Θ_i and Θ_j since all other quantities cancel. When $q_j^2 \, \overline{R_g^2} < 1.5 \, D_f$ ($R_{ij} < b_{ij}$), Eq. (16) is applicable

and we find

$$\overline{R_g^2} = \frac{a_{ij}}{k^2} \ln R_{ij} . \tag{18}$$

Somewhat larger aggregates will result in $q_j^2 \overline{R_g^2} > 1.5\ D_f$ ($R_{ij} > c_{ij}$) and $\overline{R_g^2}$ is then found by using both Eqs. (16) and (17) to formulate R_{ij}. In this event, it becomes necessary to solve the transcendental equation

$$\left(q_i^2 \overline{R_g^2}\right) \exp\left[-\frac{q_i^2 \overline{R_g^2}}{1.5\ D_f}\right] = \left[\frac{R_{ij}}{d_{ij}}\right]^{2/D_f} \tag{19}$$

The values of the quantities a_{ij}, b_{ij}, c_{ij}, and d_{ij} are defined in general terms in Table I where they are also tabulated for $\Theta_i = 45°$ and Θ_j equal to either 90° or 135° for a fractal dimension $D_f = 1.8$. Two determinations of $\overline{R_g^2}$ yielded by the use of two sets of dissymmetry ratios provide replication of this datum, but they do not afford independent information about the aggregate population. In the data analysis given below, we report the average of the two values of $\overline{R_g^2}$ found from the dissymmetry ratios R_{12} and R_{13}.

We find the volume mean diameter by dividing Eq.(10) by (13) and using Eq.(7) to eliminate $\overline{n^2}$ in favor of f_n and $\overline{n^1}$. The result is

$$D_{3o} = \frac{\lambda}{\pi} \left[\frac{4\pi E(m)\, Q_{vv}^A\ (\Theta_i)}{f_n\, F(m)\, f\,(q_i^2 \overline{R_g^2})\, K_{abs}^A}\right]^{1/3} \tag{20}$$

From Eqs. (5) and (20) for f_v and D_{3o} we find N_a which can be expressed as

$$N_a = \frac{3k^3\ f_v}{4\pi x_{3o}^3} \tag{21}$$

where $x_{30} = \pi D_{30}/\lambda$.

When $q_i^2 \overline{R_g^2} << 1$, Eq. (13) reduces to the expression applicable to Rayleigh-size spheres even though the particles are actually aggregates of small spheres. In this particular case, $\overline{R_g^2}$ and d_p do not appear in the equations, and their values cannot be determined from the above measurements.

Although the values of f_v, D_{so}, and N_a are yielded by the extinction-scattering measurements, no direct information on whether the observed particles are spheres or aggregates is provided. Independent observations are then required in order to determine the actual particle morphology. Without this added information the determination of S_t is impeded.

Data Analysis and Discussion

The flame burner which is described elsewhere [1] consisted of two coannular brass tubes of 11.1 and 101.6 mm i.d.; ethene flows through the central tube at the rate of 3.85 cm^3/s while the air flow is 713 cm^3/s corresponding to the nonsooting (NS) flame previously described[1]. In this experiment a laser light scattering apparatus is used to determine the local extinction K_{ext} and the volumetric scattering cross sections Q_{vv} (Θ_i) at Θ_i = 45°, 90°, and 135°. These quantities were measured as a function of height along a soot particle path in the annular region of high soot concentration in the coannular laminar flame. In the following analysis we take advantage of three bodies of experimental data - the scattering-extinction measurements[1], the laser velocity data[7], and observations of primary particle size obtained by thermophoretic sampling and TEM examination[8,11]. The availability of this information for the ethene diffusion flame allows the soot field to be examined along a soot particle path which, owing to the action of thermophoresis, does not coincide with a gas streamline in the lower portion of the flame where velocities are lower and thermal gradients are large. In addition, the velocity data provides a conversion of height above the burner, z, to time and allows differentiation of certain quantities to obtain rate data.

The quantity $\bar{\mathcal{H}}$ contains a ratio of higher moments of the aggregate PDF about which only limited information is available. The values of f_n and $\bar{\mathcal{H}}$ are not independent as both are influenced by the width of the aggregate PDF. We have therefore analyzed the data by treating $\bar{\mathcal{H}}$ and f_n as quantities to be adjusted to give the best agreement between d_p based on optical measurements using Eq.(9) and from TEM observations. The values of D_{so} and N_a are independent of $\bar{\mathcal{H}}$ and are weakly influenced by f_n, while d_p is sensitive to f_n and to $\bar{\mathcal{H}}$ that has a broader range of variation. On the other hand, the quantities f_v and $\overline{R_g^2}$ are calculated without reference to $\bar{\mathcal{H}}$.

The values of d_p obtained from Eq. (9) are also influenced by the refractive index m that is used in the analysis of this data. For a given value of m, we find a unique value of the product ($f_n \bar{\mathcal{K}}$) that yields the minimum rms of [d_p (TEM) - d_p (opt)] = C_r. In Table II, we list the optimum values of the product ($f_n \bar{\mathcal{K}}$), and also the individual values of f_n and $\bar{\mathcal{K}}$ that are mutually consistent with a single value of the geometric mean standard deviation σ_g for a discrete log normal distribution. Three commonly quoted values of refractive index[17,18,19] are used in this analysis. In Table II we find incompatible values of f_n and $\bar{\mathcal{K}}$ result when m = 1.57 - i0.56. On the other hand, when the recent value[19] of m = 2.10 - i0.55 is used, f_n = 1.3 and $\bar{\mathcal{K}}$ = 3.1 are found to be mutually consistent with a narrow distribution, σ_g = 0.15. This combination of parameters was selected to obtain the data used in Figures 1 to 4 for which C_r = 18%.

Recently it has been reported[20] that the value of m depends on the hydrogen content of the soot. We have explored this possibility by treating the imaginary portion of the refractive index to be height dependent to simulate the annealing action of the hot flame gases. The imaginary portion of the refractive index m_2 is allowed to vary linearly with height z and achieves the value of the m_2 = 0.55 near the tip of the flame (z = 80mm). The results of this assumption are shown in the last line in Table II where the quoted values of f_n and $\bar{\mathcal{K}}$ are consistent with a more plausible width of the distribution function, σ_g = 0.30. This treatment of the data also yields lower values of $\bar{n}^1$, and values of N_a that monotonically decrease with time as is expected when cluster-cluster aggregation is present as a growth mechanism. These interesting results are regarded as tentative and point to a future direction for research.

Figure 1 shows the values of N_a and D_{3o} obtained from Rayleigh theory and from aggregate theory plotted against height. At t_1= 25 ms the quantity $f(q_i^2 \overline{R_g^2})$ is equal to unity and the two methods give the same values for these two properties. The differences between the values of D_{3o} and N_a that are predicted by the two methods is significant at all other heights.

The quantities f_v, D_{3o}, and N_a are displayed in Figure 2, and the quantities R_g, D_{3o}, d_p(TEM), and $\bar{n}^1$ are given in Figure 3. These quantities follow a consistent pattern. The soot volume fraction f_v increases during the region where surface growth dominates (25 < t < 56 ms) and then decreases as particle oxidation occurs. Both D_{3o} and d_p parallel this trend. The aggregate number concentration N_a generally decreases as would occur if aggregation continues in the presence of either

surface growth or oxidation of the primary particles. The average number of primary particles per aggregate $\overline{n^1}$ and the mean square radius of gyration $\overline{R_g^2}$ increase as a result of cluster-cluster aggregation. Primary particle concentration N_p is not shown but is found to remain close to $10^{+19}cm^{-3}$ for all t.

The particle surface area, S_t, calculated using $\overline{n^1}$, N_a, and d_p (TEM) is shown in Figure 4. Also displayed is the value of S_t were it to be calculated on the basis that the particles are spheres rather than aggregates. It is apparent that the predicted surface areas differ by a factor of two to four. This difference is quite significant in the evaluation of the surface growth rates and points to the importance of accounting for the aggregate structure of the particles.

From the aggregate number concentration that is shown in Fig. 1, we calculate the aggregation rate K_a which is defined through the expression[21]

$$\frac{dN_a}{dt} = -\frac{K_a}{2} N_a^2 . \tag{25}$$

The latter equation can be rearranged as

$$K_a = \frac{2}{N_a(t_1)} \frac{d}{dt} \left[\frac{N_a(t_1)}{N_a(t)} \right], \tag{26}$$

and therefore the slope of the least-square straight line fit to the graph of the ratio $N_a(t_1)/N_a(t)$ vs. time t yields an average value of K_a. Values of K_a that result from use of the several values of refractive index are given in Table II. A value of 6.0×10^{-10} cm^3/s at 298 K is typical of spherical particles[21]. The lowest value of $K_a = 69 \times 10^{-10}$ cm^3/s (quoted in Table II) appears to be reasonable, but replication of these results is desired.

Summary and Conclusions

A data reduction method that is based on the use of optical cross sections for aggregates has been applied to measurements of local extinction and differential scattering at three angles by soot aggregates in a laminar ethene diffusion flame. As compared to the Rayleigh data reduction for spherical particles, this

method yields higher values of volume-mean diameter, a larger surface area per unit volume, and lower values of the aggregate number concentration. The analysis also provides the mean-square radius of gyration and the average number of primary particles per aggregate. Both these quantities increase monotonically with time as is consistent with the occurrence of cluster-cluster aggregation. Primary particle diameter is also obtained from the optical observations and it has been independently measured by thermophoretic sampling followed by TEM analysis. By requiring the rms difference between the two observations of primary particle size to be a minimum, we obtain information on the allowable values of refractive index. Higher values of the real portion of the refractive index give more plausible moment ratios of the size distribution of the aggregates. The present results indicate that a self-consistent interpretation of the light scattering properties of the soot aerosol is afforded by recognizing its aggregate structure. In particular, significant differences in the surface area and number concentration are observed for soot aerosols consisting of aggregates of primary particles. These differences have important ramifications in deriving chemical and physical rate data from the laser scattering extinction experiment. Furthermore, when combined with TEM analysis of the primary particles which constitute the aggregates, the present analysis provides the basis for evaluating the importance of other particle properties such as refractive index. Thus, this method of data analysis provides a more detailed and comprehensive description of the development and character of the soot aggregate population in laminar diffusion flames.

Acknowledgements

This work was supported by the Center for Fire Research of the National Institute of Standards and Technology, under grant numbers 60NANB6D0643 and 60NANB7D0706 and the Air Force Office of Scientific Research, Air Force Systems Command, USAF under grant number AFOSR-87-0145. One of the authors (R. A. D.) received partial support from the Center for Chemical Technology of the National Institute of Standards and Technology during a recent sabbatical leave. The assistance of Mr. Michael Carrier of NIST with aspects of the computations is acknowledged with appreciation.

Appendix I. Relationship Between d_p and $\overline{R_g^2}$ For Polydisperse Aggregates

For a polydispersion of aggregates, the mean square radius of gyration is defined by

$$\overline{R_g^2} = \frac{\sum_n R_g^2(n)\, n^2\, p(n)}{\sum_n n^2\, p(n)} \tag{A1}$$

and from Eqs. (2), (4) and (A1), it follows that

$$d_p = \frac{D_{3\,0}^3}{\overline{\mathcal{K}}\ \overline{R_g^2}} \tag{A2}$$

where

$$\overline{\mathcal{K}} = \frac{\sum_n n^2\ p(n) \sum_n n\ p(n)}{\sum_n \left[\frac{n}{k_f}\right]^{2/D_f} n^2\ p(n)} . \tag{A3}$$

When $D_f = 2.0$, Eq. (A3) reduces to

$$\overline{\mathcal{K}} = k_f \frac{\bar{n}^1\, \bar{n}^2}{\bar{n}^3} . \tag{A4}$$

The value of the prefactor k_f was found through computer simulations[9] to be 5.8. For narrow size distributions $\overline{\mathcal{K}} \rightarrow k_f$, while for discrete log normal distributions of moderate width $\overline{\mathcal{K}}$ is near 1.8 when $D_f = 1.8$. An examination of two aggregate samples, which were taken in the ethene diffusion flame[12] at a height $z = 15$ mm above burner, yields $f_n \approx 1.8$ and $\overline{\mathcal{K}} \approx$ 1.5 to 1.7, in general agreement with calculations based on a discrete log normal PDF.

Appendix II. Correction of Observed Extinction to Obtain the Volumetric Rayleigh Absorption Cross Section

For aggregates of moderate size, $q^2\overline{R_g^2}$ about equal to unity or larger, the measured extinction contains, in addition to absorption which dominates in the case of the smaller aggregates, a significant contribution owing to scattering. The extinction can be expressed

$$K_{ext} = K_{abs} \ (1 + \overline{\rho_{sa}}) \tag{A5}$$

where $\overline{\rho_{s\,a}}$ is the ratio of the scattering cross section to the absorption cross section. The latter is given by [13]

$$\overline{\rho_{sa}} = f_n \ \overline{n^1 \omega_p} \ g\,(k^2 \overline{R_g^2}) \tag{A6}$$

where ω_p, the albedo of the primary particle, is given by

$$\omega_p = \frac{2}{3} x_p^3 \ \frac{F(m)}{E(m)} \tag{A7}$$

and the function $g(k^2\overline{R_g^2})$ given by

$$g\,(k^2 \overline{R_g^2}) = \left[1 + \frac{4}{3D_f} \ k^2 \ \overline{R_g^2} \right]^{-D_f/2} . \tag{A8}$$

From Eqs. (4) and (A2) the first moment of the aggregate size distribution can be expressed by

$$\overline{n^1} = \overline{\mathfrak{N}} \ \frac{\overline{R_g^2}}{d_p^2} . \tag{A9}$$

The ratio of scattering to extinction $\overline{\rho_{sa}}$ can be calculated using TEM observations of d_p and the values of $\overline{R_g^2}$ found using the observed disymmetry ratios, R_{12} and R_{13}. With specified values of $\overline{\mathfrak{N}}$ and f_n, the quantities $\overline{n^1}$, ω_p, g and $\overline{\rho_{s\,a}}$ can be calculated. In the non-smoking ethene flame, the value of $\overline{\rho_{s\,a}}$ is as high as 30% in the midflame region where the primary particles are 33 nm in diameter. Thus, the peak values of soot volume fraction f_v are reduced by about 30% below the value which would be predicted by the conventional Rayleigh analysis for spheres in which a contribution to extinction by scattering is not included.

References

1. Santoro, R. J., Semerjian, H. G., and Dobbins, R. A., *Comb. and Flame*, **51**, 203 (1983).

2. D'Alessio, A., Dilorenzo, A., Borghese, A., Beretta, F., and Masi, S., *Sixteenth Symposium (International) on Combustion*, p. 695, The Combustion Institute, Pittsburgh, PA (1977).

3. Haynes, B. S. and Wagner, H. Gg., *Ber. Bunsenges Phys. Chem.*, **84**, 499 (1980).

4. Kent, J. H., Jander, H. and Wagner, H. Gg., *Eighteenth Symposium (International) on Combustion*, p. 113, The Combustion Institute, Pittsburgh, PA (1981).

5. Santoro, R. J., Semerjian, H. G., Emmerman, PJ., and Goulard, R., *Int. J. Heat and Mass Trans.*, **24**, 1139 (1981).

6. Dobbins, R. A., Santoro, R. J., and Semerjian, H. G., in Combustion Diagnostics by Nonintrusive Methods, T. D. McCay and J. A. Roux, Eds., Progress in Astronautics and Aeronautics, **92**, 208 (1984).

7. Santoro, R.J., Yeh, T.T., Horvath, J.J., and Semerjian, H.G., *Comb. Sci. and Tech.*, **53**, 89 (1987).

8. Dobbins, R. A. and Megaridis, C. M., *Langmuir*, **3**, 254 (1987).

9. Mountain, R. D. and Mulholland, G. W., *Langmuir*, **4**, (1988).

10. Megaridis, C. M. and Dobbins, R. A., *Twenty-Second Symposium (International) on Combustion*, p. 353, The Combustion Institute, Pittsburgh, PA (1988).

11. Megaridis, C. M. and Dobbins, R. A., *Comb. Sci. and Tech.*, **66**, 1 (1989).

12. Megaridis, C. M. and Dobbins, R. A., *to appear in Comb. Sci. and Tech.*.

13. Dobbins, R. A. and Megaridis, C. M., to appear in *Applied Optics*, See also Proceedings of the 2nd International Symposium on Optical Particle Sizing, Tempe, AZ, March 1990.

14. Jullien, R. and Botet, R., Aggregation and Fractal Aggregates, *World Scientific*, Singapore (1987).

15. Schaefer, D. W., *MRS Bulletin*, XIII, 22 (1988).

16. Botet, R. and Jullien, R., *Annales de Physique*, **13**, 153 (1988).

17. Dalzell, W. H. and Sarofim, A. F., *Journal of Heat Transfer*, **91**, 100 (1969).

18. Lee, S. C. and Tien, C. L., *Eighteenth Symposium (International) on Combustion*, p. 1159, The Combustion Institute (1981).

19. Vaglieco, B. M., Beretta, F., D'Alessio, A., private communication.

20. Habib, Z. G. and Vervisch, P., *Comb. Sci and Tech.*, **59**, 261 (1988).

21. Hinds, W.C., Aerosol Technology, Wiley and Sons, New York (1982).

Table I. Value of Constants for Use in the Determination of the Mean Square Radius of Gyration from Eqs. (18) and (19) for $\Theta_i = 45°$, and $\Theta_j = 90°$ or 135° when $D_f = 1.80$

	r_{ij}	a_{ij}	b_{ij}	c_{ij}	d_{ij}
ij = 12	0.5412	2.121	1.890	3.020	3.039
ij = 13	0.4142	1.061	2.108	4.886	4.916

The above quantities are defined by

$$r_{ij} = \sin(\Theta_i/2) \Big/ \sin(\Theta_j/2) \qquad a_{ij} = 0.75 \Big/ \left[\sin^2 \frac{\Theta_j}{2} - \sin^2 \frac{\Theta_i}{2}\right]$$

$$b_{ij} = \exp\left[0.5 D_f \left(1 - r_{ij}^2\right)\right] \qquad c_{ij} = (r_{ij})^{-D_f}$$

$$d_{ij} = c_{ij}/C_p \qquad C_p = (1.5\ D_f / e)^{D_f/2}$$

Table II. Values of f_n, $\bar{\aleph}$ and K_a recovered from minimization of fractional RMS of [d_p (TEM) - d_p (opt)] for selected values of refractive index, m at λ = 514.5 nm.

m	Ref.	$f_n\bar{\aleph}$	f_n	$\bar{\aleph}$	σ_g^*	K_a
1.57 - i0.56	17	10.1	1.0	10.1	—	490 x 10^{-10} cm^3/s
1.90 - i0.55	18	5.46	1.1	5.0	~0.05	180 "
2.10 - i0.55	19	3.93	1.3	3.1	~0.15	96 "
2.10 - i m_2^{**}	–	3.19	1.7	1.9	~0.30	69 "

*Values of geometric mean standard deviation σ_g are estimated from discrete log normal distributions which yield the indicated values of f_n and $\bar{\aleph}$.

**Imaginary portion of the refractive index m_2 is allowed to vary linearly with height in the flame to achieve 0.55 near the tip of the flame.

List of Figures

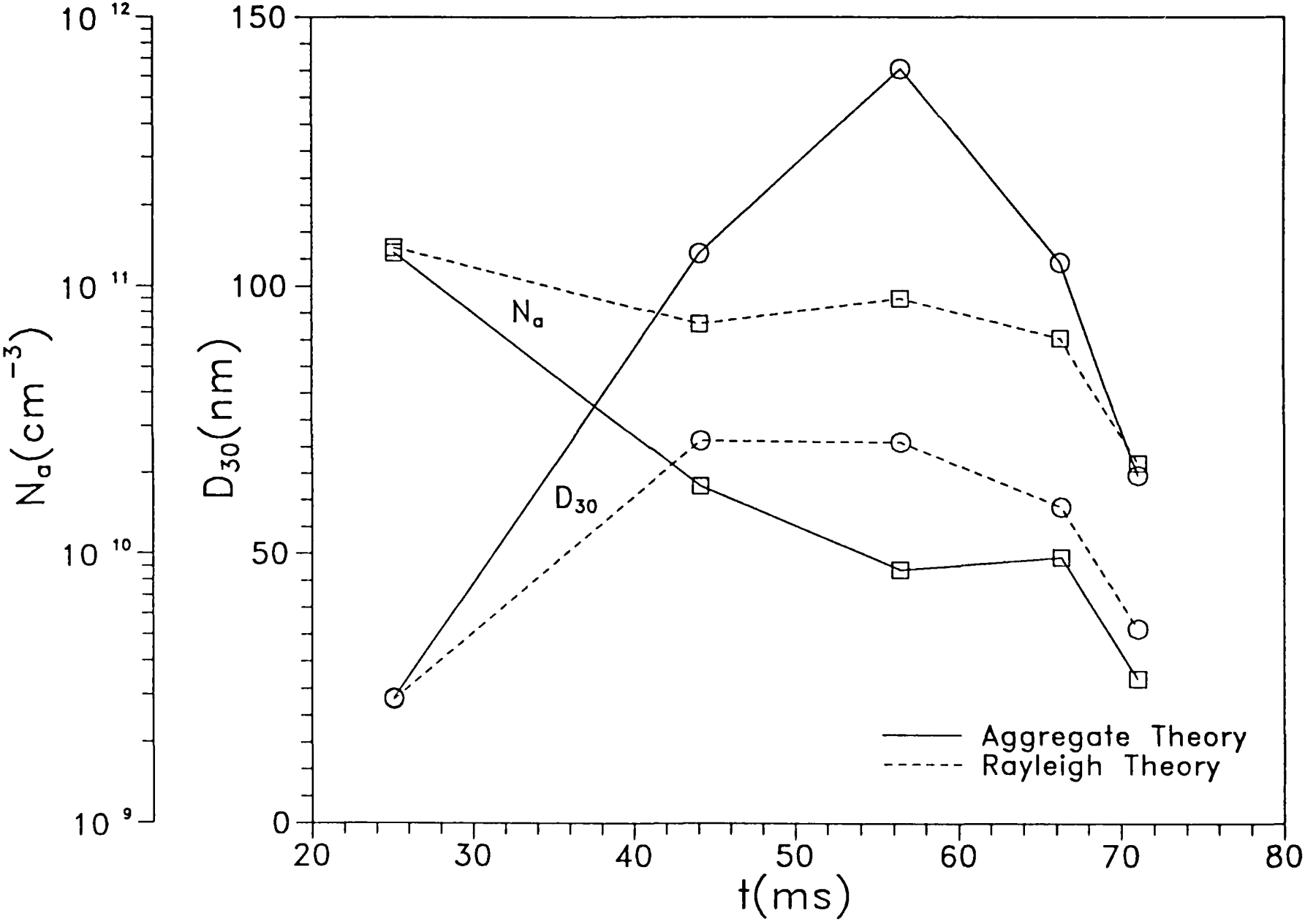
10^{12}
10^{11}
10^{10}
10^{9}
$N_a(cm^{-3})$
150
100
50
0
$D_{30}(nm)$
N_a
D_{30}
Aggregate Theory
Rayleigh Theory
20
30
40
50
60
70
80
t(ms)

Fig 1

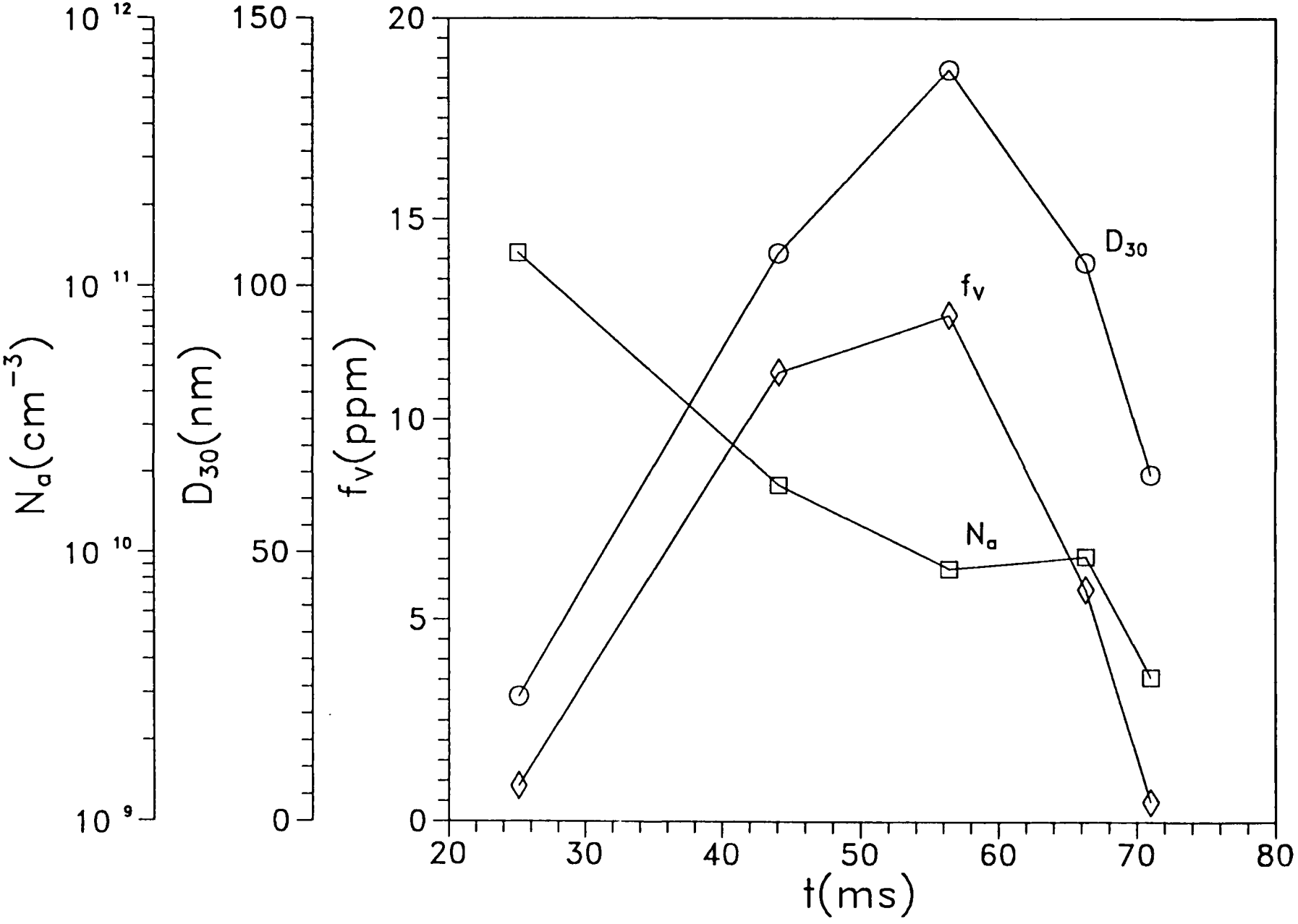
10^{12}
10^{11}
10^{10}
10^{9}
$N_a(cm^{-3})$
150
100
50
0
$D_{30}(nm)$
20
15
10
5
0
$f_v(ppm)$
20
30
40
50
60
70
80
t(ms)
D_{30}
f_v
N_a

Fig. 2

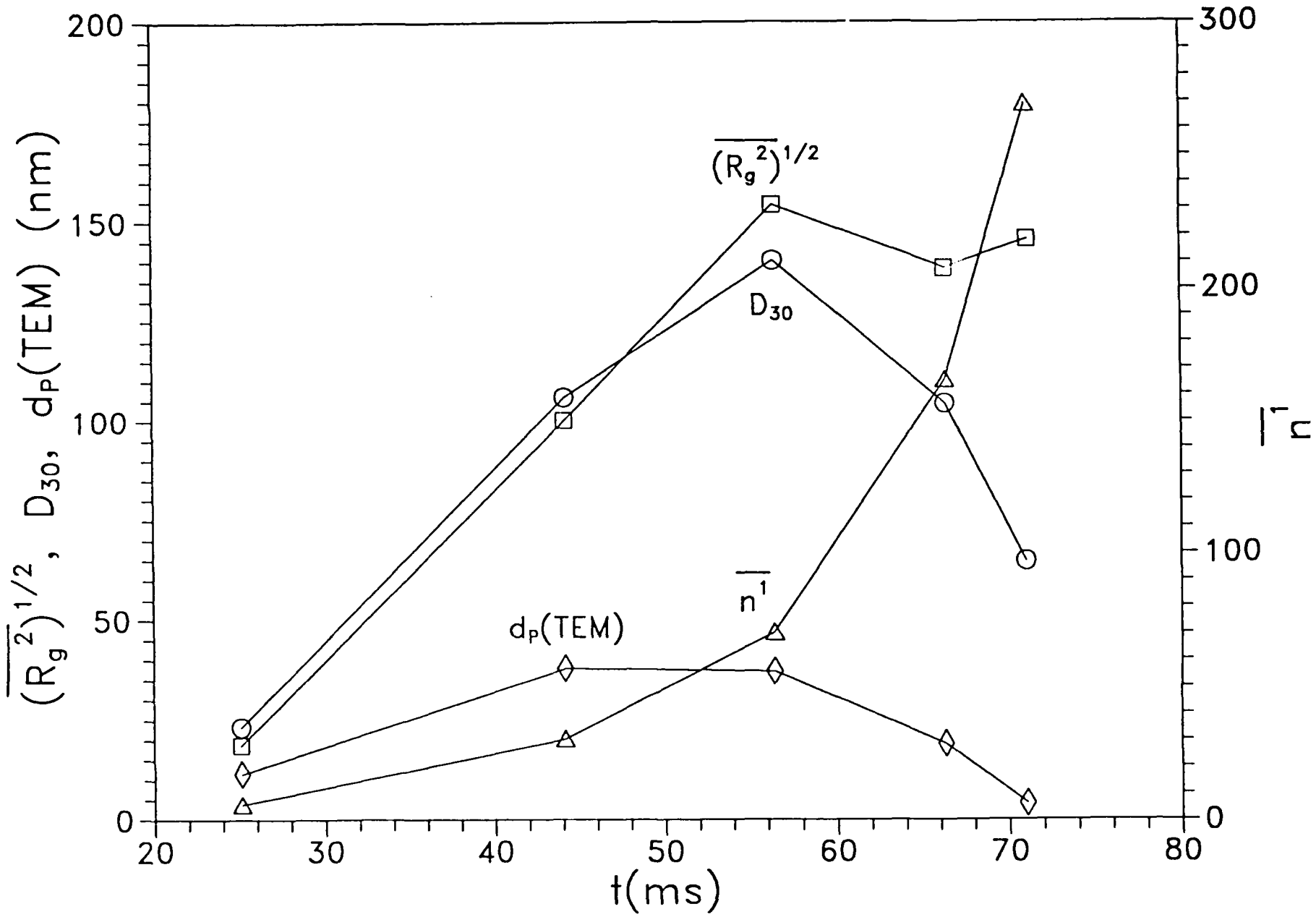
200
150
100
50
0
300
200
100
0
20
30
40
50
60
70
80
t(ms)
$\overline{(R_g^2)}^{1/2}$, D_{30}, d_P(TEM) (nm)
$\overline{n^1}$
$\overline{(R_g^2)}^{1/2}$
D_{30}
d_P(TEM)
$\overline{n^1}$

Fig 3

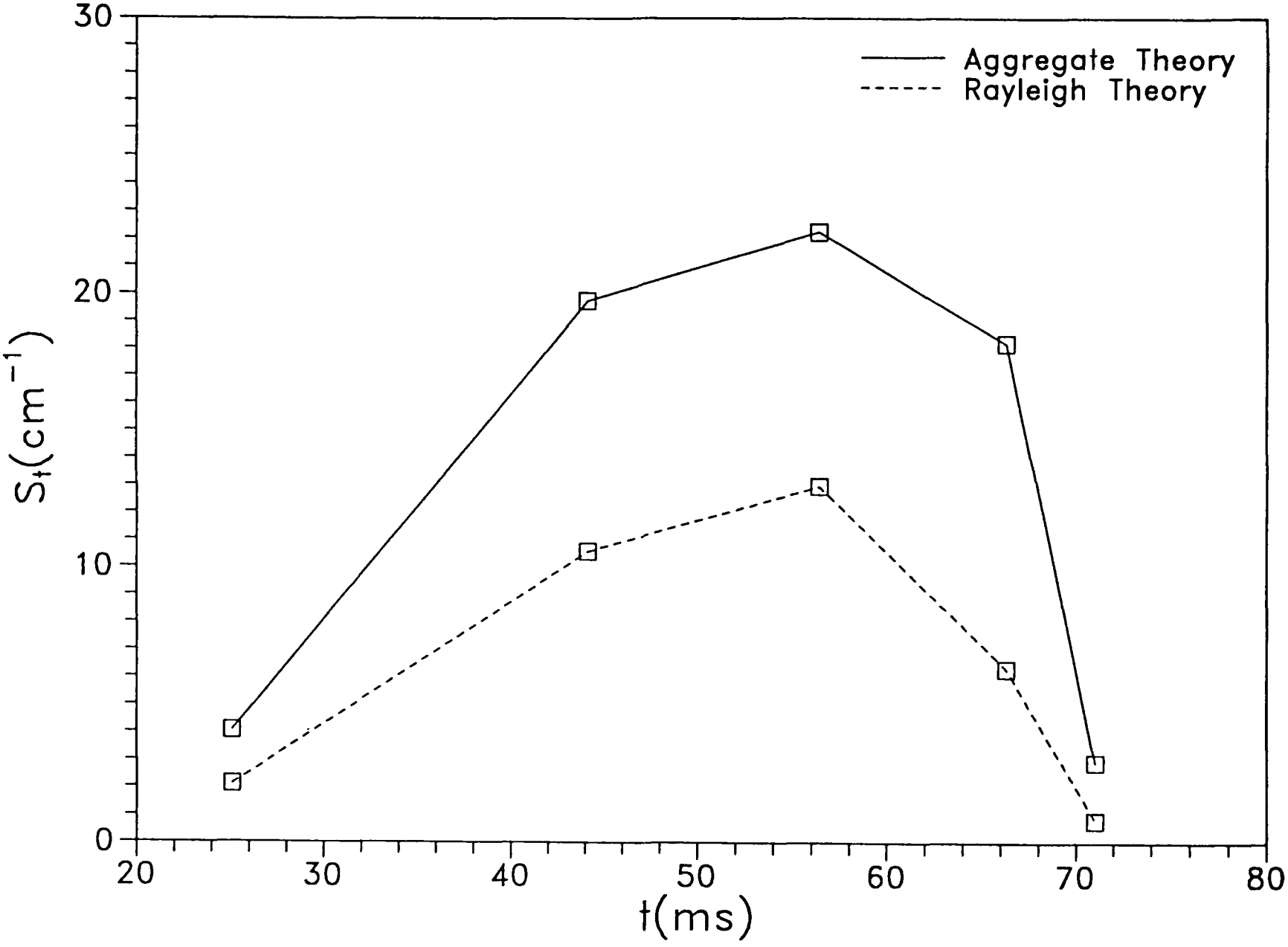
Aggregate Theory
Rayleigh Theory
$S_t(cm^{-1})$
t(ms)
0
10
20
30
20
30
40
50
60
70
80

Fig. 4

Attachment 2

Isolation of Byoyancy Effects in Jet Diffusion Flame Experiments
by
R. W. Davis, E. F. Moore, R. J. Santoro and J. R. Ness

(submitted to Combustion Science and Technology)

ISOLATION OF BUOYANCY EFFECTS IN JET DIFFUSION FLAME EXPERIMENTS

R.W. Davis and E.F. Moore, Center for Chemical Technology, National Institute of Standards and Technology, Gaithersburg, MD 20899

R.J. Santoro and J. Ness, Department of Mechanical Engineering, The Pennsylvania State University, University Park, PA 16802

ABSTRACT

Buoyancy plays a crucial role in the dynamic behavior of jet diffusion flames. In order to determine the exact role that buoyancy plays, a simple procedure is described for varying in isolation the relative buoyancy force in stationary laboratory jet diffusion flame experiments. This procedure, which is derived from a theoretical model of these flames, merely requires that background pressure be varied while maintaining constant mass flows of fuel and oxidizer into the burner. It is shown that the sole result of these pressure variations in the theoretical model is that the effective gravitational acceleration acting upon the flame varies as the square of the pressure. Comparisons are made between the structure of a low speed laboratory methane/air flame at various pressures and the results of a direct numerical simulation of the same flame with various gravitational accelerations. Similar evolutions in flame structure are observed in both cases.

INTRODUCTION

Investigations into the dynamic structure of jet diffusion flames have become more common in the last decade [Yule et al. (1981), Eickhoff and Winandy

(1985), Roquemore et al. (1989), Takahashi et al. (1988), Chen et al. (1988)]. This is because these geometrically-simple flames exhibit many features which are generic to more complex combusting flows. The interactions between the flame surface and outer surrounding vortex structures are of particular concern, especially in low speed and transitional (buoyancy-dominated) jet diffusion flames. It is these interactions which are apparently responsible for various forms of flame flicker [Chen et al. (1988), Roquemore et al. (1989), Buckmaster and Peters (1986)]. Since the outer vortex structures form in a buoyancy-driven shear layer outside the flame surface, it becomes highly desirable to vary the buoyancy force (relative to inertial and viscous forces) in isolation from all other parameters in order to observe the resulting effects, especially on flame flicker. However, this has been difficult and expensive to do, requiring accelerating test rigs. It is the purpose of this paper to outline a more practical procedure for isolating buoyancy effects in experiments involving jet diffusion flames.

The procedure to be described here is derived from a theoretical model for jet diffusion flames based on the flame sheet and conserved variable approximations. It will be shown that buoyancy effects in this model can be isolated by simply maintaining constant mass flows into the burner while varying the background pressure. In order to test the validity of this procedure, results obtained from numerical solutions of the equations of motion are compared with experimental results obtained in a pressure chamber. A similar evolution in tip-cutting behavior is observed both numerically and experimentally as pressure increases, albeit at different pressure levels due presumably to stability differences between the two flames. Previous experimental investigations of jet diffusion flames at varying pressures have focused on the structural effects of

Reynolds number variations in the excited case [Strawa and Cantwell (1988)] or on soot formation [Flower (1988)]. The present study is believed to be the first investigation of these flames to focus solely on isolating buoyancy effects. It is not, however, the purpose of this paper to thoroughly document these effects but instead to open the door to future more exhaustive studies.

THEORETICAL BACKGROUND

The nondimensional continuity, momentum and state equations for the unsteady axisymmetric flow of a multicomponent fuel jet surrounded by a coflowing airstream are

$$\frac{\partial \rho}{\partial t} + \nabla\cdot(\rho \underset{\sim}{q}) = 0, \tag{1}$$

$$\rho \frac{\partial \underset{\sim}{q}}{\partial t} + \rho(\underset{\sim}{q}\cdot\nabla)\underset{\sim}{q} = -\nabla \tilde{p} - \rho \mathrm{Ri}\hat{e}_z + \frac{1}{\mathrm{Re}}\{-\nabla \times [\mu (\nabla \times \underset{\sim}{q})] + 4/3\ \nabla (\mu \nabla\cdot \underset{\sim}{q})\}, \tag{2}$$

$$\rho\ T \sum_i R_i\ Y_i = p_o = R_{air}\ . \tag{3}$$

Here ρ is density; μ is viscosity; T is temperature; $\underset{\sim}{q} = (u,v)$, where u and v are velocity components in an axisymmetric reference frame (r,z); Y_i is the mass fraction of species i with gas constant R_i; and $\hat{e}_z$ is the unit normal in the axial direction. The pressure consists of a constant background pressure, p_o, plus a perturbation pressure, $\tilde{p}\ (r,z,t)$, where $p_o > > \tilde{p}$. As discussed by Rehm and Baum (1978), the omission of $\tilde{p}$ from Eq. (3) is entirely appropriate here, resulting in the suppression of acoustic waves while admitting the low frequency motions due to buoyant effects. All quantities in Eqs. (1-3) have been

nondimensionalized with respect to conditions in the coaxial airstream at the burner inlet. Thus Re = Reynolds number = $\frac{U_o L}{\nu_o}$ and Ri = Richardson number = $\frac{gL}{U_o^2}$, where U_o and ν_o are the entering airstream velocity and kinematic viscosity; L is the fuel jet radius; and g is gravitational acceleration.

In order to reduce the complexity of the problem while still providing a good approximation to the physical situation, a flame sheet model (infinite rate kinetics) will be employed here. In addition, the Lewis number (ratio of thermal to species diffusivities) is assumed to be unity. Therefore, conserved variables, β_i, for species mass fractions and enthalpy can be utilized. These obey the simple nondimensional convection-diffusion equation

$$\frac{\partial(\rho\beta_i)}{\partial t} + \nabla \cdot (\rho \underset{\sim}{q}\, \beta_i) = \frac{1}{Pe} \nabla \cdot (\rho D \nabla\beta_i), \tag{4}$$

where D is binary diffusion coefficient and Pe = Peclet number = $\frac{U_o L}{D_f}$, with D_f taken as the diffusion coefficient of fuel into nitrogen at the burner inlet. The conserved variables are defined as

$$\beta_1 = \frac{\alpha Y_{ox} + Y_f^I - Y_f}{\alpha Y_{ox}^I + Y_f^I},$$

$$\beta_2 = \frac{h - h_{ox}^I + \frac{Y_f Q}{\alpha}}{\frac{Y_f^I}{\alpha} Q + h_f^I - h_{ox}^I}.$$

Here h is enthalpy; Q is heat release per unit mass of oxygen consumed; $\alpha = \frac{\nu_f M_f}{\nu_{ox} M_{ox}}$, where ν is stoichiometric coefficient and M molecular weight; subscripts f and ox refer to fuel and oxidizer (with nitrogen accounted for in the enthalpy); and superscript I refers to burner inlet conditions. The analytical model for the jet diffusion flame under discussion here consists of

Eqs. (1-4) along with appropriate boundary conditions. A flame sheet exists at locations where $\beta_1 = Y_f^I/(\alpha Y_{ox}^I + Y_f^I)$. The solution method will be discussed in the next section. The remainder of the discussion here will focus on the overall characteristics of the model.

It is apparent from Eqs. (1-4) that, given a fixed set of boundary conditions, the solution field is dependent upon only three parameters: Re, Ri, and Pe. Of particular concern here is the Richardson number, Ri, which represents the ratio of buoyancy forces to inertial forces. By varying this parameter independently, it is possible to isolate the effects of a varying relative buoyancy force (or gravitational acceleration) on the theoretical jet diffusion flame. If the model here is assumed to be a good approximation to reality, then this isolation of buoyancy effects could also be performed experimentally if Ri could be independently varied in the laboratory. A procedure for accomplishing this will now be discussed.

A simple method for varying Ri while keeping Re, Pe and the boundary conditions fixed is merely to maintain constant mass flow of both fuel and air into the burner while varying the background pressure. Since $\rho_o U_o$ is fixed and μ_o is pressure independent, Re will remain constant under this procedure. Both U_o and D_f vary inversely with pressure, thus maintaining a fixed Pe. However, Ri will vary as the square of the pressure. Since the other thermophysical properties inherent in the model (specific heats, Lewis number) can be assumed independent of pressure, this variation in Ri is the <u>only</u> effect of the background pressure changes. Thus, the effective gravitational acceleration will vary as pressure squared, e.g., a background pressure of 2 atmospheres corresponds to 4 g's. This relationship is the basis of this paper and will be investigated both computationally and experimentally. It is reasonable to

believe that, at least over a moderate range of pressure changes, this procedure can provide a simple means of varying the relative buoyancy force in these flames without resorting to expensive moving test rigs.

NUMERICAL MODEL

The analytical model consisting of Eqs. (1-4) and appropriate boundary conditions is solved numerically by means of a modified version of the finite difference scheme employed previously by Davis and Moore (1985) to simulate cold mixing layer dynamics. This scheme employs a variably-spaced staggered mesh in which pressures are defined at cell centers and normal velocities at cell faces. Quadratic upwind differencing is used for convection, and an explicit Leith-type of temporal differencing is employed. At each time step, a Poisson equation for perturbation pressure is solved by a direct method. Variable thermophysical properties are calculated as described by Mitchell (1980), and no turbulence or radiation models are employed. Species binary diffusion is taken as fuel into nitrogen inside the flame and oxygen into nitrogen outside. All relevant variables are specified at the burner inlet ($z = 0$); axisymmetry is enforced along the burner centerline; and zero or constant gradients are employed at very large axial and radial distances (i.e., no shroud). Mesh dimensions are 5000 fuel jet radii axially (145 mesh cells) and 50 radially (84 cells), both attained by employing rapidly expanding mesh cell sizes away from the flame. Run times on the NIST CYBER 205 are typically several hours, with initial solution fields obtained by means of a steady-state flame simulation [Davis and Moore (1987)]. After awhile, flame flickering commences in the unsteady computation without the

triggering required in the cold jet case [Davis and Moore (1985)]. The numerical model just described has also been used to study the dynamic structure of propane/air jet diffusion flames, the results of which have compared well with experimental visualizations [Davis et al. (1989)].

EXPERIMENTAL APPARATUS

The experimental portion of this study was conducted in a high pressure diffusion flame burner (Fig. 1) designed for operation at pressures up to twenty atmospheres. The coannular burner employed here consists of a fuel tube of 1.10 cm inner diameter surrounded by a 10.16 cm inner diameter air passage. The air passage is partially filled with glass beads followed by a series of fine mesh screens to provide for flow conditioning of the incoming air. A honeycomb section 2.54 cm in thickness with 0.15 cm square cells is located at the burner exit to provide a uniform exit air flow field. The fuel tube, which extends 0.25 cm above the ceramic honeycomb, is also partially filled with glass beads for flow conditioning.

The burner is housed in a high presure chamber which consists of two cylindrical sections. The lower section is constructed of 20.32 cm nominal diameter pipe (8 inch diameter, schedule 40 carbon steel pipe) which is 61 cm in length. This section houses the motorized translational stage which provides for vertical movement of the burner. Electrical connections as well as gas lines for the air and fuel are introduced through a flange located on the bottom of this section. The bottom flange is attached to a ball bearing stage which supports the weight of the entire chamber. Horizontal movement of the chamber can thus be

achieved using a small motorized translation stage. Both the horizontal and vertical movements of the burner are controlled by stepper motors which are interfaced to a laboratory personal computer. For the present study only the vertical motion capability was required.

The upper section of the chamber contains four 6.35 cm diameter windows which are 1.27 cm in thickness and are at the same axial height 90° apart. These windows provide access for high speed video recording as well as laser diagnostic measurements. This section is constructed of a 76.2 cm long, 15.24 cm nominal diameter pipe (6 inch diameter, carbon steel pipe). The thicker wall pipe (2.19 cm) is required to maintain the proper material strength after machining the holes for the windows. The operating pressure for the burner is controlled using manual valves located on a flange mounted to the top of the pressure chamber. Steady operating pressures over a range of one to twenty atmospheres can be maintained in the system.

Gas flows are measured using a mass flow metering system. For the fuel flow rates, a mass controller is utilized which maintains the mass fuel flow rate constant regardless of the chamber pressure. The air flow rate is monitored using a mass flow meter and, thus, the air flow has to be manually adjusted to maintain a constant mass flow rate for the air as the chamber pressure is varied.

In the present study methane was burned with air supplied from an in-house compressor capable of providing 300 SCFM of air at 300 psig pressure. These capabilities exceed the pressure and flow rate requirements for this study. Prior to introducing the air into the burner it is passed through filters to remove particles and moisture. Methane is supplied from high pressure cylinders with a purity of 99%.

High speed video recording of the flame structure was obtained using a Spin

Physics high speed video camera operated at a 500 Hz framing rate. Observations of the flame were made through one of the four windows located in the chamber and provided a two inch open aperture viewing region. The flame structure images were obtained using the soot luminosity of the flame. Since the flame dimensions typically exceeded the two inch viewing area provided by the window, the burner was raised or lowered to an appropriate region of interest for study. In some cases a series of video sequences was required to characterize the entire flame. The Spin Physics camera also provides the capability to play back the recorded images at slow speeds or a single frame at a time. This capability was used in the analysis of the recorded images which follows.

RESULTS AND DISCUSSION

As a test of the aforementioned procedure for varying the relative buoyancy force in jet diffusion flames, a coordinated series of computations and experiments has been carried out. The selected configuration was a methane/air diffusion flame with fuel and air burner inlet velocities of 10 and 20 cm/sec, respectively, and a fuel jet radius of 0.55 cm. This flame appears virtually steady at atomospheric pressure while entering into a simple tip-cutting mode at higher pressures. This mode is quite regular in frequency and extremely reproducible in terms of the flame structures which result. The flame is observed to periodically pinch off at a particular axial height, with the cut-off tip being convected upward while the lower region recedes. The lower part of the flame subsequently increases in length and the cycle repeats. When viewed in real time, this periodic tip-cutting appears as a flickering flame. Due to the

low flow velocities involved, buoyancy is clearly an important factor in this flame's behavior, while small-scale turbulence is almost certainly not. The low level of soot production minimizes radiative losses, and the Lewis number can reasonably be assumed as unity. Thus, for all these reasons, this flame was deemed to be a suitable candidate for the present study.

Experiments involving this methane/air flame have been carried out at pressures ranging from 1 to 8 atmospheres. In these experiments the mass flow rates of the fuel and air were maintained constant as the chamber operating pressure was increased. Thus, the volumetric flow rates and linear velocities at the burner exit were proportionately reduced. Corresponding computations have been performed by simply varying the gravitational acceleration in the model as the square of this background pressure; i.e., $Ri \sim p_o^2$, where $Ri = 1.35$ for $p_o = 1$ atm. The results are summarized in Table I, with the evolution in flame structure as a function of p_o (or Ri) shown in Fig. 2. This figure compares recorded images of the experimental flame at four pressures with computed flame sheets (solid squares) and their surrounding vortex structures visualized via isovorticity contours. It can be seen that the experimental and computational evolutions of flame structure with increasing pressure are strikingly similar. The computational evolution, however, occurs at lower pressures, a subject which will be discussed subsequently. The flame structure seen at low pressure (1 atm experimentally; 0.5 atm computationally) in Fig. 2a is essentially steady, although there is slight tip wavering in both cases. The flame height, H, is slightly larger computationally, and some weak outer vortices can be seen near the tip. At the higher pressures (1.5 atm experimentally; 0.75 atm computationally) of Fig. 2b, tip-cutting has begun in both cases. The tip-cutting height, H_s, is slightly greater computationally, while the computed tip-

cutting frequency, f, is slightly less. The external vortex structures have strengthened and moved downward as compared with Fig. 2a. This is due to the increased buoyancy-induced velocity gradients at this pressure, with the effective gravitational acceleration here being greater than that for Fig. 2a by a factor of 2.25. At the next higher pressure (2 atm experimentally; 1.2 atm computationally), the cut-off tip has assumed a basically triangular shape with a cusped region flaring out from its base. Both the experimental and computational tip-cutting heights have decreased from Fig. 2b, with the outer vortices also moving down commensurately. The experimental frequency, but not the computational one, has dropped slightly. The situation at even higher pressure (3 atm experimentally; 1.41 atm computationally) is illustrated in Fig. 2d. The base of the cut-off tip has straightened out to produce a highly triangular shape. The tip-cutting heights have dropped again, the frequencies are about the same, and the outer vortex structures are somewhat lower. It is clear from both Table I and Fig. 2 that the experimental evolution of flame structure with increasing pressure compares well with the evolution computed via Richardson number increases, thus tending to confirm the basic validity of the buoyancy-isolation procedure at issue here.

Although comparisons between numerical and experimental results have been made for a pressure range of one to three atmospheres, high speed video recordings have been obtained for pressures as high as eight atmospheres. Comparisons are limited to the lower range of pressures because three-dimensional effects become significant at pressures near and above four atmospheres, thus rendering comparisons with the axisymmetric model of little value. This loss of axisymmetry in the experimental flame is most evident in the evolution of the upper section of the flame after a "tip-cutting" event has occurred. Under all

pressure conditions where flickering is observed, the luminous cut-off region is observed to disappear with time. This is due to the oxidation of the soot particles which are responsible for the observed luminosity. For the pressure range of one to three atmospheres, this process is observed to proceed in a regular, symmetric manner with the lowest regions of the cut-off tip oxidizing first. As the pressure is raised to four atmospheres and above, the rapid oxidation process is observed to favor one side of the cut-off tip and to proceed diametrically upward and across this upper flame structure. At pressures between five and six atmospheres, the upper flame structure is actually split into two or four sections depending on the chamber pressure. In each case, these observations are highly reproducible from cycle to cycle and clearly demonstrate the strengthening of azimuthal instabilities with rising pressure. This increasing instability, however, is precisely the type of behavior that would be expected as Ri increases, as found by Subbarao (1989) in experimental studies of buoyant helium jets. It is also noted that the addition of full three-dimensionality to the model employed here would in no way affect the conclusions previously reached concerning the relationship between background pressure variations and the relative buoyancy force.

Finally, the lower pressures (or effective gravitational accelerations) found in the computational evolution in Fig. 2 require some explanation. This is probably due to the use of the flame sheet approximation and the lack of any radiation in the model, thus resulting in higher temperatures computationally than experimentally. This, in turn, should lead to higher velocities and sharper gradients in the computed flame than in the experimental one, thus rendering the former more unstable. Thus it should require less effective gravitational acceleration to trigger a particular stage of the structural evolution process

computationally than experimentally.

CONCLUSIONS

A simple procedure has been described for isolating buoyancy effects in jet diffusion flame experiments. All that is necessary is that background pressure be varied while maintaining constant mass flows of fuel and oxidizer into the burner. A theoretical model for these flames indicates that this procedure isolates Richardson number (or relative buoyancy force) as the only variable parameter, which is equivalent to varying the gravitational acceleration. A joint series of experiments and computations involving a pressurized low speed methane/air diffusion flame has provided strong evidence to support the theory.

It is clear that much work needs to be done in order to clarify the important role that buoyancy plays in jet diffusion flame dynamics. The results presented here only open the door to future studies, which can now be performed with reasonable effort and cost-effectiveness. Future research is also needed in order to determine the limits of usefulness of the buoyancy-isolation procedure described here. Clearly use of this procedure to attain very small effective gravitational accelerations appears unreasonable, as chemical kinetics could certainly not be ignored at the low pressures required. However, relaxation of the requirement that Lewis number be unity appears feasible since the Prandtl and Schmidt numbers can both be considered as independent of pressure. Finally, since the basic model described here is not dependent on a particular geometry, other types of diffusion flames in different burner configurations could also be considered as candidates for buoyancy-isolation experiments. Thus, the possibilities for future research efforts in the area of buoyancy effects in

diffusion flames appear rather substantial.

ACKNOWLEDGEMENT

Two of the authors (RJS and JN) wish to gratefully acknowledge the sponsorship of the Air Force Office of Scientific Research, Air Force Systems Command, USAF, under grant number AF 87-0145.

REFERENCES

Buckmaster, J., and Peters, N. (1986). The infinite candle and its stability - a paradigm for flickering diffusion flames. Twenty-First Symposium (International) on Combustion, The Combustion Institute, p. 1829.

Chen, L.-D., Seaba, J.P., Roquemore, W.M., and Goss, L.P. (1988). Buoyant diffusion flames. Twenty-Second Symposium (International) on Combustion, The Combustion Institute, p. 677.

Davis, R.W., and Moore, E.F. (1985). A numerical study of vortex merging in mixing layers. Phys. Fluids 28, 1626.

Davis, R.W., and Moore, E.F. (1987). Numerical modeling of steady laminar diffusion flames. Paper No. 15 presented at the Twentieth Fall Technical Meeting of the Eastern Section of the Combustion Institute, National Bureau of Standards, Gaithersburg, MD, November 2-5, 1987.

Davis, R.W., Moore, E.F., Chen, L.-D., Roquemore, W.M., Vilimpoc, V., and Goss, L.P.. Preliminary results of a numerical/experimental study of the dynamic structure of a buoyant jet diffusion flame. Submitted to Comb. and Flame.

Eickhoff, H., and Winandy, A. (1985). Visualization of vortex formation in jet diffusion flames. Comb. and Flame 60, 99.

Flower, W.L. (1988). An investigation of soot formation in axisymmetric turbulent diffusion flames at elevated pressure. Twenty-Second Symposium (International) on Combustion, The Combustion Institute, p. 425.

Mitchell, R.E. (1980). A theoretical model of chemically reacting recirculating flows. Report No. SAND79-8236, Sandia National Laboratories, Livermore, CA.

Rehm, R.G., and Baum, H.R. (1978). The equations of motion for thermally driven, buoyant flows. Jour. of Research of the Nat. Bur. Stds. 83, 297.

Roquemore, W.M., Chen, L.-D., Goss, L.P., and Lynn, W.F. (1989). The structure of jet diffusion flames. in Borghi, R. and Murthy, S.N.B. (Eds.), Turbulent Reactive Flows, Lecture Notes in Engineering, Springer-Verlag, Berlin, Vol. 40, p. 49.

Strawa, A.W., and Cantwell, B.J. Investigation of an excited jet diffusion flame at elevated pressure. Submitted to J. Fluid Mech..

Subbarao, E.R. (1989). The effects of Reynolds number and Richardson number on the structure of a vertical co-flowing buoyant jet. AIAA Paper No. 89-1800.

Takahashi, F., Mizomoto, M., and Ikai, S. (1988). Structure of the stabilizing region of a laminar jet diffusion flame. J. Heat Trans. 110, 182.

Yule, A.J., Chigier, N.A., Ralph, S., Boulderstone, R., and Ventura, J. (1981). Combustion-transition interaction in a jet flame. AIAA Jour. 19, 752.

TABLE I

Experimental/Numerical Comparison of Tip-Cutting Heights and Frequencies

Pressure, p_o (atm)		Tip-Cutting Height, H_s (cm)		Frequency, f (Hz)	
Experiment	Computation	Experiment	Computation	Experiment	Computation
1.0	0.50 (Ri=0.34)	H=8	H=10	Steady	Steady
1.5	0.75 (Ri=0.76)	8	9	18.5	15
2.0	1.20 (Ri=1.94)	6	7	15	15
3.0	1.41 (Ri=2.70)	4	6	16	15

FIGURES

1. Schematic representation of high pressure diffusion flame burner.

2. Comparisons between experimentally recorded images and computational flames (solid squares with surrounding isovorticity contours) at four values of background pressure. (a) experimental p_o = 1.0 atm; computational p_o = 0.5 atm. (b) experimental p_o = 1.5 atm; computational p_o = 0.75 atm. (c) experimental p_o = 2.0 atm; computational p_o = 1.2 atm (d) experimental p_o = 3.0 atm; computational p_o = 1.41 atm.

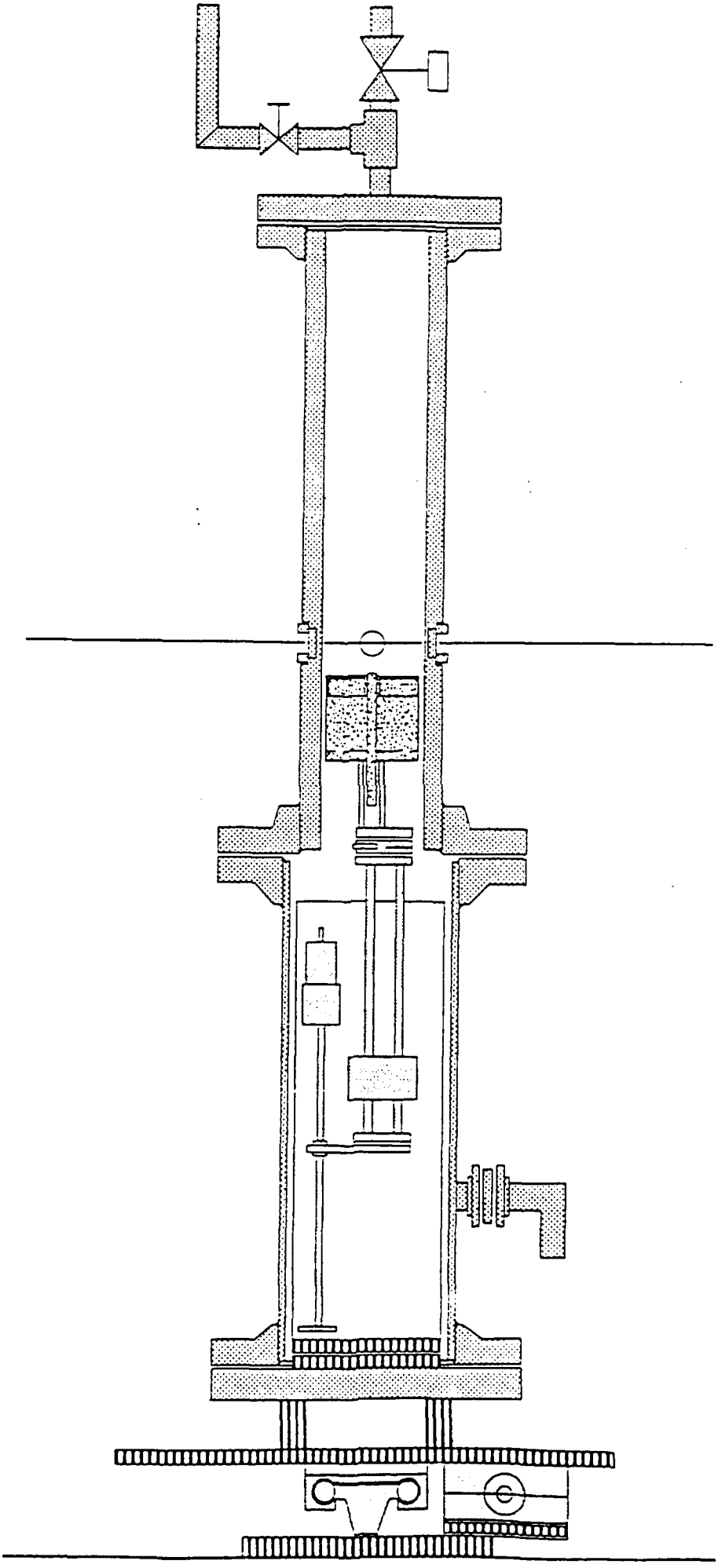

Fig. 1

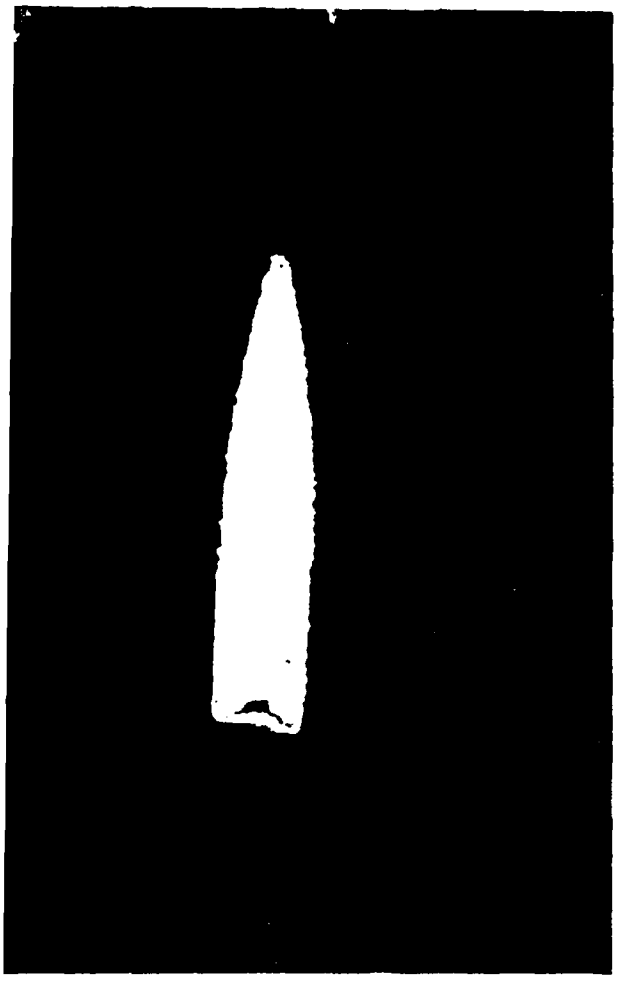

a.

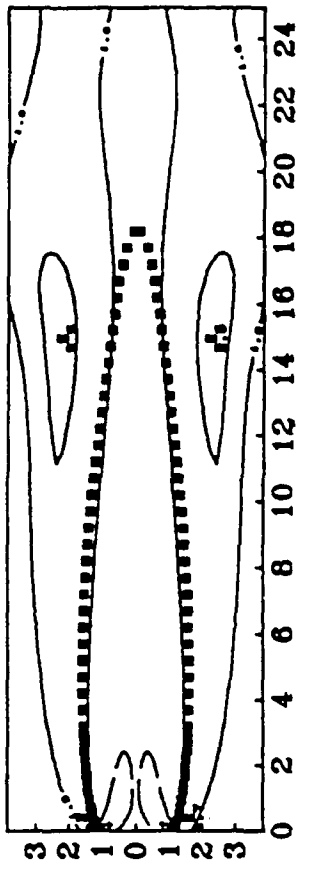
0 2 4 6 8 10 12 14 16 18 20 22 24
3 2 1 0 1 2 3

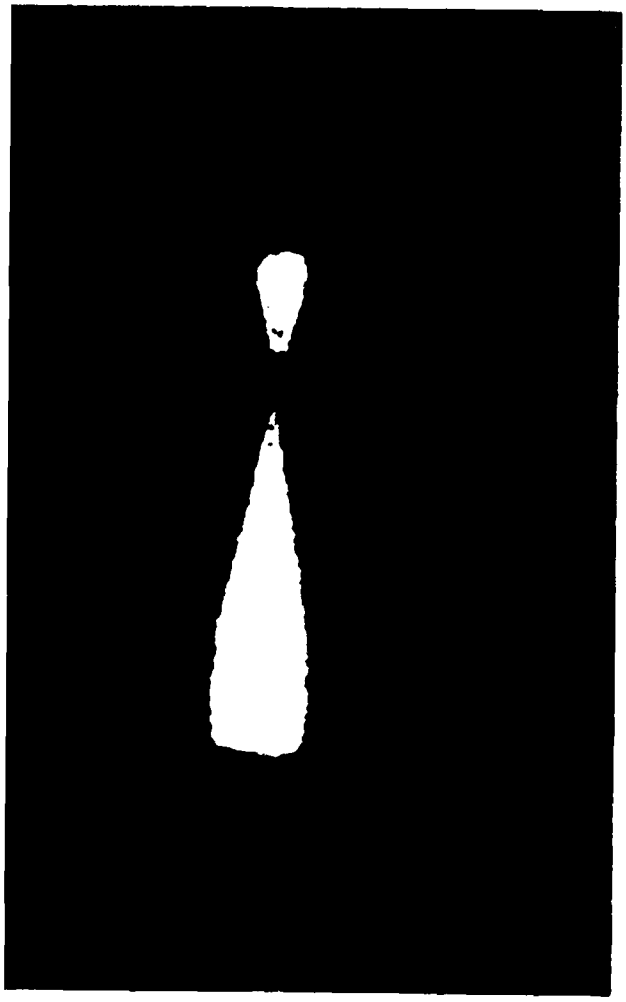

b.

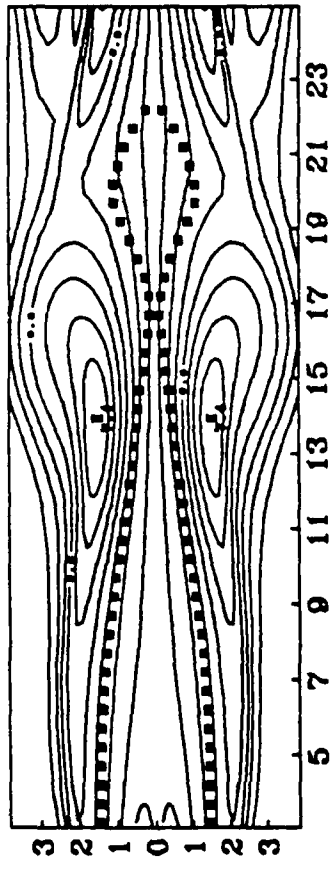
5 7 9 11 13 15 17 19 21 23
3 2 1 0 1 2 3

Fig. 2

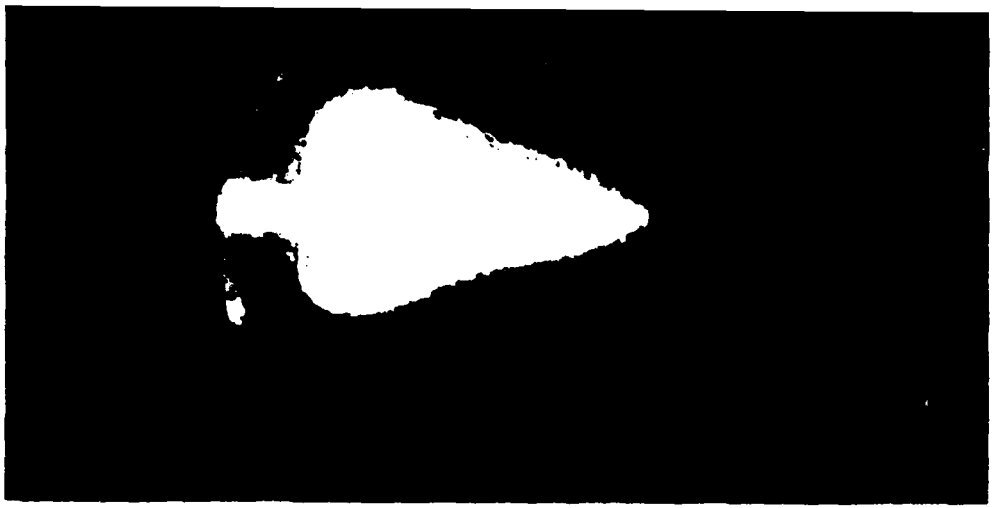

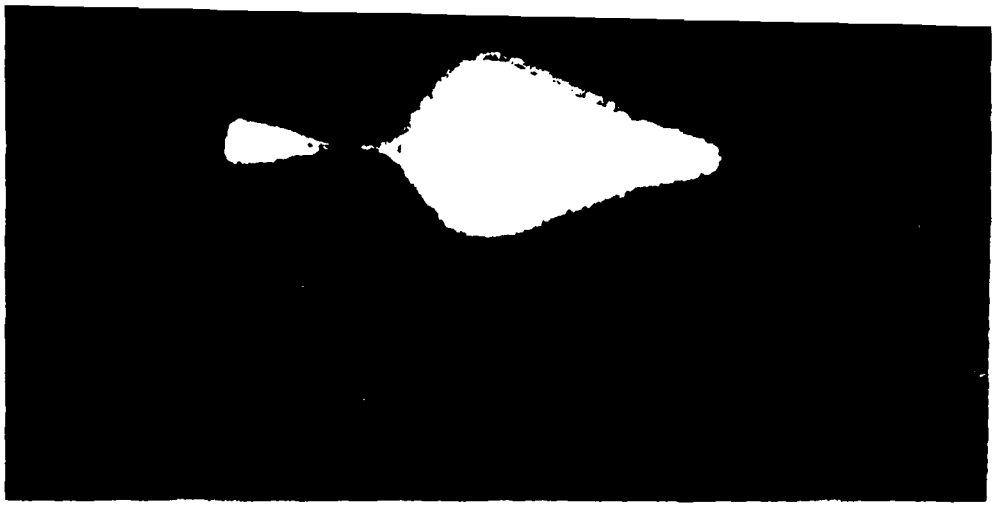

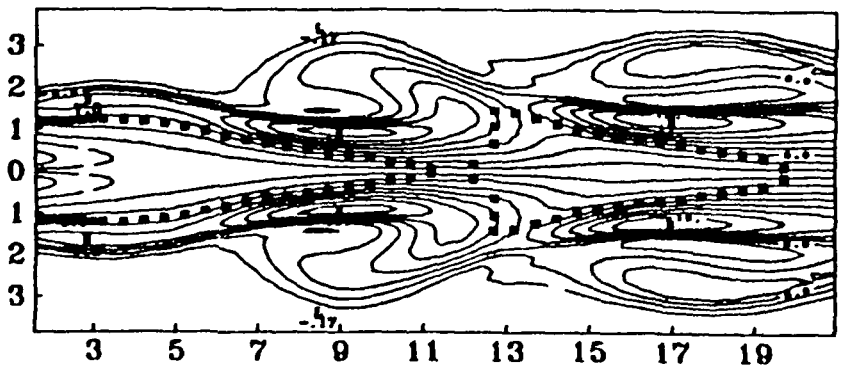

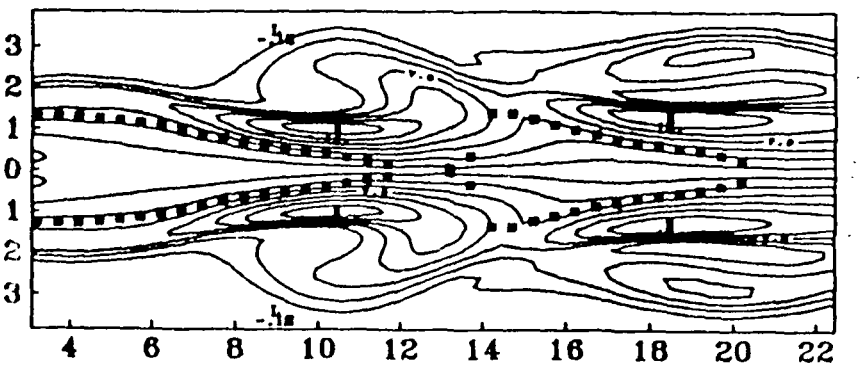

Fig. 2